A Boolean network model of hypoxia, mechanosensing and TGF-β signaling captures the role of phenotypic plasticity and mutations in tumor metastasis

Short title:

Boolean model of hypoxia, mechanosensing and TGF-β signaling in cancer

Authors:

Grant Greene[1], Ian Zonfa[1,2], Erzsébet Ravasz Regan[1]*

Affiliations:

[1] Biochemistry and Molecular Biology, College of Wooster, Wooster, OH 44691, U.S.A.

[2] Uniformed Services University of the Heath Sciences, Bethesda, MD, 20814, U.S.A.

* Corresponding Author

Abstract

The tumor microenvironment aids cancer progression by promoting several cancer hallmarks, independent of cancer-related mutations. Biophysical properties of this environment, such as the stiffness of the matrix cells adhere to and local cell density, impact proliferation, apoptosis, and the epithelial to mesenchymal transition (EMT). The latter is rate-limiting step for invasion and metastasis, enhanced in hypoxic tumor environments but hindered by soft matrices and/or high cell densities. As these influences are often studied in isolation, the crosstalk between hypoxia, biomechanical signals, and the classic EMT driver TGF-β is not well mapped, limiting our ability to predict and anticipate cancer cell behaviors in changing tumor environments. To address this, we built a Boolean regulatory network model that integrates hypoxic signaling with a mechanosensitive model of EMT, which includes the EMT-promoting crosstalk of mitogens and biomechanical signals, cell cycle control, and apoptosis. Our model reproduces the requirement of Hif-1α for proliferation, the anti-proliferative effects of strong Hif-1α stabilization during hypoxia, hypoxic protection from anoikis, and hypoxia-driven mechanosensitive EMT. We offer experimentally testable predictions about the effect of VHL loss on cancer hallmarks, with or without secondary oncogene activation. Taken together, our model serves as a predictive framework to synthesize the signaling responses associated with tumor progression and metastasis in healthy vs. mutant cells. Our single-cell model is a key step towards more extensive regulatory network models that cover damage-response and

senescence, integrating most cell-autonomous cancer hallmarks into a single model that can, in turn, control the behavior of in silico cells within a tissue model of epithelial homeostasis and carcinoma.

Author Summary

The cellular environment in and around a tumor can aid cancer progression by promoting several cancer hallmarks. This environment can affect growth and cell death, as well as a phenotype change that renders cells migratory and invasive: the epithelial to mesenchymal transition. Hypoxia (low oxygen availability) is known to promote this transition, while the attachment of cells to soft matrices or high cell density environments hinders it. These influences are often studied in isolation. As a result, their crosstalk is poorly understood. To address this, we have built a network model of cellular regulation that integrates a cell's responses to hypoxia, the biophysical environment, and growth signals to model cell division, death, and the epithelial to mesenchymal transition in environments cells encounter during metastatic tumor progression. Our model reproduces a wide range of experimental cell responses and offers experimentally testable predictions about the emergence of cancer hallmarks driven mutations that affect the hypoxic response. Our single-cell model is a key step towards more extensive cell-scale models that also include cell aging and damage response. These, in turn, can serve as building blocks of a larger tissue model of healthy vs. cancerous epithelia.

Introduction

Tumor formation is marked by the development of mutations leading to dysregulated cell growth and death. Accumulation of cancer hallmarks is further aided by the tumor microenvironment (TME) – the biochemical composition, biophysical structure of the tissue, and non-cancer cells residing inside and around a tumor, all of which exert a major influence on the development and progression of cancer (1,2). The TME is both variable and dynamic, with primary and secondary metastatic sites found to have differing environments that further vary by cancer origin (3–5). Interestingly, the TME can contribute to the initial formation of tumors, rather than simply relying on stochastic genetic change as originally believed for carcinogenesis (6). As cancer remains the second leading cause of death globally, understanding the unique conditions that promote metastasis contributing to 70-90% of cancer mortality is paramount to identifying therapeutics to both prevent and treat it (7).

A rate limiting step for metastasis is epithelial to mesenchymal transition (EMT), a process where cells gain mesenchymal characteristics and lose their apical-basal polarity; aiding their migration, tissue invasion, and dissemination to secondary sites (8). Yet, the reverse process (MET) is also crucial for tumor growth at secondary sites (9,10). EMT and MET often do not require mutations to arise; rather they emerge due to the phenotypic plasticity of cancer cells responding to the TME. The stepwise process of EMT is controlled by two central double-negative feedback loops (11,12). The first switch flips when an epithelial cell transitions to a

85 hybrid E/M state, requiring the activation of SNAI1 by extracellular signals,
86 accompanied by repression of the epithelial microRNA miR-34 (13). In this hybrid
87 E/M state, cells lose their apical-basal polarity, become migratory, yet still maintain
88 adherens junctions with neighbors to facilitate collective migration. To complete full
89 EMT, loss of the second epithelial microRNA, miR-200, must occur in conjunction
90 with high expression of the EMT factor ZEB1 (14). This leads to the loss of E-
91 cadherin and all adherens junctions, prompting a full mesenchymal phenotype.
92 While these two feedback loops are but a small part of the regulatory network
93 driving EMT, their central role is illustrated by the fact that hybrid E/M states were
94 first predicted by a computational model of this circuit (11,12), later confirmed *in*
95 *vitro* (15–18) and *in vivo* (19–22). A series of computational models of increasing
96 complexity followed, exploring the role of phenotypic stability factors (23,24), the
97 connection between hybrid E/M cells and cancer stemness (18), spatial patterning
98 in tumors (25), and the role of biological noise in EMT (26). Most relevant for this
99 study are models that capture the crosstalk between multiple EMT-driving
100 extracellular signals (27). Among these, the influential large Boolean model by
101 Steinway et al. integrated TGFβ, Wnt, Notch, Hedgehog, and serval growth
102 signaling pathways, predicting and verifying several interventions capable of
103 controlling EMT *in vitro* (28,29).
104
105 In addition to well-characterized transforming signals such as TGFβ secreted by
106 nearby cells, EMT is influenced by two key aspects of the TME. First, the
107 concentration of oxygen is known to decrease in response to tumor growth (30).
108 The increased size of solid tumors coupled with poor vascularization and vessel

109 integrity lead to hypoxia – defined as an oxygen supply of < 40 mmHg or < 6% O_2
110 (31,32). Tumor cells respond to hypoxic conditions with the secretion Vascular
111 Endothelial Growth Factor (VEGF) to induce angiogenesis and fulfil their oxygen
112 demand (33,34). Yet, blood vessel formation within tumors is highly dysregulated
113 and ineffective at relieving hypoxia (32,35). Acute, moderate hypoxia, in turn,
114 promotes invasion and metastasis – an alternative pathway for tumor cells to
115 resolve the oxygen demand by migrating to oxygen rich tissue. Second, EMT is
116 highly dependent on the biophysical environment. Namely, high cell density hinders
117 EMT (36,37), while the increased matrix stuffiness characteristic of fibrotic tissue
118 promotes it (38,39). Both hypoxia and the biophysical environment were shown to
119 contribute to immuno-, radio- and chemotherapy resistance, furthering cancer
120 mortality (40–44). However, the context-dependent crosstalk of hypoxia and the
121 biophysical environment in driving EMT and MET are not well understood.
122
123 The hypoxic response occurs through two mechanisms: a canonical response
124 mediated transcriptionally by Hypoxia Inducible Factor (HIF) proteins, and a non-
125 canonical loss of oxygen-dependent degradation enzyme function, increasing the
126 stability of target proteins (31,45–47). HIF proteins are heterodimeric transcription
127 factors comprised of an oxygen-sensitive Hif-α domain paired with a constitutively
128 stable Hif-β domain. Regulation of the Hif-α subunit occurs through the oxygen-
129 dependent hydroxylation of its proline residues, performed by prolyl hydroxylase
130 domain (PHD) enzymes (**Fig. 1A**) (48). This in turn allows for recognition by E3
131 ubiquitin ligase Von Hippel Lindau protein (pVHL), leading to rapid Hif-1α
132 degradation (49). Additionally, the Factor Inhibiting HIF (FIH) hydroxylase enzyme

133 uses O_2 as a substrate for asparagine hydroxylation, inhibiting HIF binding to
134 transcription co-activator p300 and thus blocking its transcriptional activity (50).
135 Most higher eukaryotes have three oxygen-sensitive HIFα isoforms; Hif-1α, Hif-2α,
136 and Hif-3α (51). The first discovered and most well understood subunit is Hif-1α,
137 stabilized in response to acute hypoxic stress (52). In contrast, Hif-2α is
138 preferentially stabilized during long-term hypoxic reprogramming, offering temporal
139 control over HIF regulation (53,54). Finally, Hif-3α forms a negative feedback-loop
140 with Hif-1α to fine-tune long-term hypoxia, while maintaining its own unique
141 transcriptional activity (55,56). In comparison to the ubiquitously expressed Hif-1α,
142 Hif-2α and -3α are more temporal and cell-specific (51,57,58).
143
144 Since the discovery of Hif-1α, several hundred genes have been discovered to be
145 differentially expressed under hypoxia as a result of HIF transcription, affecting a
146 wide array of signaling pathways (59–61). Critically, both mesenchymal factors
147 SNAI1 and ZEB1 are transcriptional targets of Hif-1α (62,63). Additionally, several
148 other mesenchymal markers are shared targets Hif-1α and the classical EMT-
149 inducing TGF-β pathway (64,65). Independent of HIF transcriptional regulation,
150 non-canonical hypoxia responses involving the loss of oxygen-dependent PHD
151 hydroxylation and the accumulation of reactive oxygen species (ROS) through the
152 electron transport chain were also shown to promote EMT. For example, PHD/pVHL
153 has been implicated in repressing Transforming Growth Factor-β (TGF-β),
154 contributing to increased TGF-β expression under hypoxia (66). Moreover, ROS
155 accumulation caused by increased glycolysis under hypoxia contributes to Src
156 activation and PHD inhibition, furthering invasion, metastasis, apoptosis resistance,

157 and treatment resistance (67–69). Src tyrosine kinase activity upregulates ERK
158 (70) and is required for loss of cadherin-dependent cell-cell contacts under hypoxia
159 (71).
160
161 Despite the delineation of molecular pathways responsible for canonical and non-
162 canonical hypoxic responses, downstream effects on the cell can appear
163 paradoxical. For example, the Hif-1α-driven Warburg effect is required for
164 proliferative metabolism (72), yet extreme hypoxia can inhibit proliferation (73,74).
165 While metabolic reprogramming under chronic hypoxia aids proliferation (75), acute
166 stabilization of Hif-1α under hypoxia has been shown to prevent proliferation
167 through strong Myc antagonization (74). Similarly, while hypoxia induces apoptosis,
168 hypoxia-driven EMT confers resistance to anoikis (apoptosis triggered by loss of
169 adhesion) (76,77). The pro- and anti-apoptotic effects of hypoxia are suggested to
170 be distinguished by severity and length, governed by two competing cellular
171 compartments: the cytosol vs. mitochondria. On one hand, hypoxia-driven loss of
172 mitochondria membrane potential and decreased ATP production can increase
173 mitochondrial membrane permeability, resulting in cytochrome C release and
174 downstream caspase cleavage under severe hypoxia (78,79). Under moderate
175 hypoxia, localization of Hif-1α to the mitochondria prevents oxidative-stress
176 induced apoptosis through On the other hand, Inhibitor of Apoptotic Protein-2 (IAP-
177 2) expression increases under hypoxia, providing cytosolic prevention of apoptosis
178 independently of Hif-1α activity (80). Loss of HIF function attenuated these
179 behaviors, demonstrating the necessity of the canonical pathway.

180 These differing outcomes highlight the need to better map the precise combinations
181 of environmental conditions leading to each response. Furthermore, the effect of
182 the biophysical environment on these diverging responses remails largely
183 unexplored.
184
185 The tumor microenvironment is heterogenous, both in terms of the spatial
186 distribution of different tumor-associated cells and temporal differences in its
187 molecular composition. Thus is important to understand how the biophysical
188 environment modulates the phenotypic diversity tumor cell populations (81,82). For
189 example, single-cell sequencing experiments have found heterogeneous expression
190 of epithelial and mesenchymal markers emerging from the same tumor site,
191 confirming a broad range of states within the EMT spectrum (22,83,84). As oxygen
192 availability in tumors is also not static, it is important to understand the interplay
193 between these two highly dynamic pathways: the hypoxic response and the
194 induction of EMT in response to the biophysical environment.
195
196 The goal of this study is to map the way hypoxia alters these responses in a
197 biophysical milieu-dependent manner. In a previously published Boolean model of
198 mechanosensitive EMT, we reproduced known effects of the biophysical
199 environment on EMT and TGFβ signaling. We predicted that in the absence of TGFβ,
200 the decision between no response, partial EMT, and full EMT in mitogen-stimulated
201 epithelial cells on a stiff ECM is dictated by cell density (85). Here we expanded this
202 model by including key regulators of the canonical and non-canonical hypoxic
203 response, and integrated their effect on growth factor signaling, proliferation, EMT,

204 and apoptosis. Our model reproduces the requirement of Hif-1α for normal
205 proliferation (86), as well as the anti-proliferative effects of strong Hif-1α
206 stabilization during hypoxia (73,74). Additionally, we capture the molecular
207 mechanism of Hif-1α mediated SNAI1/2 and ZEB1 upregulation (62,87,63) and
208 reproduce hypoxia-driven EMT (63,88); independent of TGF-β (66) but dependent
209 on a stiff ECM (89). Our model also reproduces hypoxic protection from anoikis
210 (76). We offer experimentally testable predictions about the context-dependent
211 effects of TGF-β signaling on hypoxia-mediated EMT, as well as VHL loss on cancer
212 hallmarks with or without secondary oncogene activation. Taken together, we offer
213 a mechanistic, predictive framework to synthesize the signaling responses
214 responsible for hypoxic behaviors associated with tumor progression and metastasis
215 in healthy vs. mutant cells.

216 Results

217 Expression of Hif-1α is Required for Proliferation

218

219 To model the way hypoxia contributes to EMT and proliferation, we expanded
220 our previous mechanosensitive Boolean network, which includes a detailed cell
221 cycle control circuit driven by growth signaling (MAPK, PI3K/Akt and mTORC)
222 integrated with cell-cell and cell-ECM adhesion, contact inhibition, control of EMT,
223 and apoptosis (85). Here we incorporated a hypoxia module with both canonical
224 and non-canonical response mechanisms (85) (**Fig. 1A;** model in **SM File 1**). This
225 module captures the acute, moderate hypoxic response, focused on Hif-1α and its

226 downstream transcriptional activity (90). In cells, Hif-1α activation and signaling
227 has two functionally distinct regimes, requiring two Boolean nodes to properly
228 capture its effects. Moderate Hif-1α is activated in response to growth factor
229 signaling under normal O_2 conditions to boost glycolysis and proliferative
230 metabolism; we encode this as *Hif1a_basal* = ON. A stronger activation occurs in
231 response to hypoxic conditions or TGF-β signaling, typically in combination with
232 deactivation of Hif-1α inhibitors such as pVHL (modeled as *Hif1a_High* = ON). Next,
233 we included Hif-1α mediated transcription of mesenchymal markers including
234 SNAI1/2, ZEB1, LEF1, β-catenin (and its subsequent nuclear localization / complex
235 formation with Hif-1α) (46,62,63,91). **Fig. 1B** shows the three stable states (fixed-
236 point attractors) of the isolated EMT module, matching the expected activity of EMT
237 regulators in three distinct phenotypic cell states along the EMT spectrum; namely
238 epithelial (top), hybrid E/M (middle) and mesenchymal (bottom). The full network
239 is shown in **Fig. 1C**, while the Boolean rules and detailed biological justification for
240 each of the 165 nodes and 763 links is included in **SM Table 1**.
241
242 **Figure 1. The hypoxic response affects proliferative signaling and EMT. A)**
243 Regulatory module depicting the canonical and non-canonical hypoxic response,
244 along with influences from other signaling pathways and cell states. **B)** Three stable
245 attractors of the isolated EMT regulatory switch (**SM File 2**). *Orange/blue node*
246 *borders:* ON/OFF. **C)** Modular network representation of our extended Boolean
247 model. *Gray:* inputs representing environmental factors; *dark blue:* Adhesion
248 signals; *red: TGFβ* signaling; *green*: Growth Signaling (*lime green*: basal AKT &
249 MAPK, *bright green:* PI3K/AKT oscillations, *mustard*: mTORC1, *dark green: NF-κB,*
250 *GSK3, FoxO1*); *dark red:* Apoptotic Switch*; light blue:* Contact Inhibition; *pink/light*

251 *orange:* Migration; *light brown:* Origin of Replication Licensing; *lilac:* Restriction
252 Switch; *purple:* Phase Switch; *dark orange:* cell cycle processes; *yellow:* EMT switch;
253 *teal:* hypoxic response; → : activation; ⊣ : inhibition.
254
255 First, we validated our model by comparing its behavior to 150 experimental assays
256 curated from 13 primary literature papers focused on EMT and hypoxia signaling.
257 The 150 assays covered cell behaviors in response to 19 distinct protein or
258 microRNA perturbations (knockdown/ overexpression) and involved 229 unique
259 statistical tests, listed in **SM Table 2**. Our model reproduced 92% (138) of the 150
260 assays (207 of 229 statistical tests; auto-generated figures in **SM File 4**). Of the 12
261 failed assays marked in **SM Table 2**, 7 involved experiments that directly
262 contradict others on the list; the others pointed to model limitations detailed in our
263 *Discussion*. Below, we showcase key validation experiments related to hypoxic
264 signaling, along with a series of model predictions.
265
266 To test whether the updated model can reproduce the context-dependent influence
267 of Hif-1α activation on proliferation, we used synchronous Boolean update to map
268 the model's attractors in each cellular environment (*Computational Methods IV*). As
269 our starting cell state, we chose a quiescent epithelial phenotype under normoxia,
270 low mitogen exposure sufficient for quiescence, plated at moderate density (e.g., at
271 a monolayer's edge). We then exposed this cell to increasing concentrations of
272 mitogen (**Fig. 2A,** *full time-course:* **SM Fig. 1**). As Hif-1α is a transcriptional
273 inducer of glycolytic genes, we expected a moderate Hif-1α activity increase in spite
274 of the presence of oxygen, required for maintaining the energy demand associated

275 with proliferation (92–94). Indeed, our model showed intermittent, moderate Hif-1α
276 activation preceding each division (**Fig. 2A**, *arrows*). The average activity of the
277 *Hif1a_basal* node in a population under increasing mitogen exposure went up in
278 tandem with Myc, Cyclin D1 and Cyclin E (**Fig. 2B**), parallelling the increase in cell
279 cycle progression (**Fig. 2C**). Indeed, loss of Hif-1α under normoxia reduced
280 proliferation in our model (**Fig. 2D**), as demonstrated *in vitro* (86). Yet, high levels
281 of Hif-1α of accumulation was also associated with cell cycle arrest due to Myc
282 inhibition (73,74), reproduced by our model by overexpression of the *Hif1a_High*
283 node in strongly mitogen-stimulated cells (**Fig. 2E**). Strong Hif-1α activation blocks
284 the cell cycle via Myc repression, as demonstrated by partial cell cycle rescue in
285 cells with hyper-active Myc (**SM Fig. 2**). In summary, both over and under-
286 expression of Hif-1α severely limit proliferation in our model, as described in the
287 experimental literature.
288
289 **Figure 2. Hif-1α is required for proliferation under normoxia. A)** Dynamics of
290 relevant regulatory molecule expression/activity during exposure of a quiescent cell to
291 increasing mitogen signaling (60 update-steps of 45%, 65%, 85% and 100% high GF;
292 full network dynamics in **SM Fig. 1A**). *X-axis:* update steps annotated by cell cycle
293 phase (G0: quiescence; G1: start of cell cycle entry; S: DNA synthesis; G2: growth
294 phase 2; M: metaphase; A T: anaphase, telophase, cytokinesis); *y-axis*: nodes
295 organized by regulatory module; *yellow/blue*: ON/OFF; *red arrow:* Hif1a_basal node.
296 **B)** Average expression of *Hif1a_basal* (teal), Myc, CyclinD1 and CyclinE (lilac) in the
297 four consecutive time windows with increasing GF_High input (45%, 65%, 85%,
298 100%) in an ensemble of 10,000 simulations representing individual cells. **C)** Fraction
299 of time cells spend in quiescent (orange) vs. proliferative (*dark red*) states (*left*) and

300 fraction of time a cell's state matched the G0_G1, G2 or SAC state of the phase switch
301 (*right*) in subsequent time windows with increasing growth factor (45%, 65%, 85%,
302 100%) in an ensemble of 10,000 cells. **D)** Fraction of time cells spend quiescent
303 (*orange*) vs. proliferative (*dark red*) states (*left*) and fraction of time cell states match
304 the G0_G1, G2 or SAC state of the phase switch (*right*) at increasing levels of
305 *Hif1a_basal* knockdown (*autocrine TGF-β:* 5% TGFb_secr knockdown). **E)** Fraction of
306 time cells spend in quiescence (*orange*) vs. in cell cycle (*dark red*, *left*) and fraction of
307 time cell states match the G0_G1, G2 or SAC state of the phase switch (*right*) at
308 increasing levels of *Hif1a_High* hyper-activation (*log2 scale:* 0, 0.625, 1.25, 2.5, 5,
309 10, 20, 40 and 80% Hif1a_High = ON; *autocrine TGF-β:* 5% TGFb_secr knockdown).
310 *Length of time-window for continuous runs:* 500 steps (~24 wild-type cell cycle
311 lengths); *total sampled live cell time:* 100,000 steps; *update*: synchronous; *initial*
312 *condition for all sampling runs*: epithelial cells in GF:1, CellDensity_High:1,
313 Stiff_ECM:1, Trail:0, Self_Loop:1, TGFb_ext:0, Hypoxia:0; *environment of sampling*
314 *runs:* saturating growth signals (GF_High:1), moderate density (CellDensity_Low:1).

315

316 Hypoxia arrests proliferation and induces EMT

317

318 Having demonstrated the role of Hif-1α expression in proliferation under
319 normoxia, we next assessed the effect of the hypoxic response on proliferation and
320 EMT. As described above, Hif-1α overexpression in the presence of oxygen lead to
321 cell cycle arrest due to Myc repression (**SM Fig. 2**) (74). Hypoxia induced a similar
322 cell cycle arrest in our model, as lack of oxygen blocked PHD2 hydroxylation and
323 downstream VHL-mediated Hif-1α degradation (**Fig. 3A**). In addition to cell cycle

324 arrest, our simulation showed hypoxia-induced EMT in cycling cells (**Fig. 3A**), as
325 expected from experimental literature (86,89,95) . Namely, hypoxia resulted in Hif-
326 1α mediated transcription of mesenchymal transcription factors SNAI1/2, ZEB1,
327 LEF1, and nuclear β-catenin, generating a mesenchymal phenotype and complete
328 loss of epithelial markers (**SM Fig. 3A**) (63,91,96). In addition, non-canonical (Hif-
329 1α independent) stabilization of IKKα due to a lack oxygen-dependent hydroxylation
330 by PHD lead to NF-κB activation (**SM Fig. 3A**) (97).
331
332 As seen in **Figure 3A**, hypoxia triggers autocrine TGF-β signaling due to a
333 combination of oxygen dependent loss of VHL activity (66), Hif-1α mediated
334 activation of TGF-β converting enzyme furin (98), and critically, secretion of TGF-β
335 induced by EMT transcription factors (46,99). Yet, this effect is a consequence
336 rather than driver of EMT under hypoxia, as TGF-β receptor I knockdown does not
337 block hypoxia-induced EMT – though it slows it in mild hypoxia (**Fig. 3B-C**). That
338 said, lack of TGF-β signaling does weaken cell cycle arrest in the presence of
339 mitogens (**Fig. 3D**). Moreover, hypoxic EMT in VHL independent (**Fig. 3B-C**), as
340 PHD2-mediated hydroxylation and degradation of Hif-1α requires oxygen even in
341 VHL-overexpressing cells (**SM Fig. 3B**) (48,100). In contrast, TGF-β can only
342 stabilize Hif-1α in the absence of VHL (**SM Fig. 3C**) (100). As EMT transcription
343 factors induction occurs independently through either Hif-1α or SMAD2/3/4, the two
344 pathways do not rely on each other to promote EMT (**SM Fig. 3D**).
345
346 **Figure 3. Hypoxia induces EMT and blocks cell cycle independently of TFG-β**
347 **signaling. A)** Dynamics of regulatory molecule expression in a proliferating cell in

348 response to hypoxia (80 / 40 / 40 update-steps of normoxia/hypoxia/normoxia at 95%
349 saturating mitogen exposure and moderate cell density). *X-axis:* update steps
350 annotated by cell cycle phase (G0: quiescence; G1: start of cell cycle entry; S: DNA
351 synthesis; G2: growth phase 2; M: metaphase; A/T: anaphase, telophase,
352 cytokinesis); *y-axis*: nodes organized by regulatory module; *yellow/blue*: ON/OFF;
353 *black/white labels:* relevant phenotypes; *update*: synchronous. **B-C)** Fraction of time
354 cells at moderate density exposed to weak (B) or strong mitogens (C) spend in
355 epithelial (*yellow*), hybrid E/M (*dark yellow*) and mesenchymal (*mustard*) states at
356 increasing hypoxia exposure. **D)** Fraction of time strong mitogen-exposed cells spend
357 in quiescence (*orange*) vs. in cell cycle (*dark red*) at increasing hypoxia exposure. **B-**
358 **D)** *1st row:* wild-type; *2nd row*: 100% IKKα/β knockdown; *3nd row*: 100% TGFβ-RI
359 knockdown; *4th row:* 100% pVHL hyper-activation. *log_2 X axis:* 0, 0.625, 01.25, 2.5,
360 5, 10, 20 and 40 hypoxia; *black dashed line:* 80%; *white stars:* altered from wild-
361 type; *length of time-window for continuous runs:* 100 steps (~5 wild-type cell cycle
362 lengths); *total sampled live cell time:* 100,000 steps; *update*: synchronous; *initial*
363 *condition for all sampling runs*: epithelial cells in GF:1, CellDensity_Low:1,
364 Stiff_ECM:1, Trail:0, Self_Loop:1, TGFb_ext:0, Hypoxia:0; *environment of sampling*
365 *runs:* GF_High = 0.25 (B) or GF_High = 0.95 (C) and moderate density
366 (CellDensity_Low:1); *autocrine TGF-β loop:* 5% TGFb_secr knockdown.

367

368 ## The biophysical environment and oxygen availability
369 modulate epithelial to mesenchymal transition and its
370 reversal

371

372 Experimental literature on the crosstalk between the hypoxic response and
373 ECM primarily focuses on hypoxia induced remodeling by fibroblasts, or induction of
374 the Warburg effect (101–105), leaving the interplay of hypoxia and ECM stiffness or
375 cell density underexplored. One of the few direct studies on the dependence of EMT
376 on ECM stiffness under hypoxia demonstrated that mesenchymal marker induction
377 under hypoxia positively correlate with matrix stiffness in vitro[12]. To test whether
378 our model can reproduce this, we started our next simulation with a quiescent
379 epithelial cell on a soft ECM, at low density and under hypoxia (arrested due to an
380 inability to stretch as well as hypoxia). We then gradually increased ECM stiffness
381 by stochastically turning ON the *Stiff_ECM* node, until its saturation (*Stiff_ECM* =
382 ON). As shown in **Figure 4A**, mesenchymal markers gradually turned on starting
383 from *Stiff_ECM = 0.5*, and cells maintained a fully mesenchymal state by *Stiff_ECM*
384 *= 0.75* (complete time-course: **SM Fig. 4A***)*. In contrast, cells under normoxia
385 underwent partial EMT and entered the cell cycle, never reaching high levels of
386 ZEB1 to repress miR-200c and E-cadherin expression (**Fig. 4B**, **SM Fig. 4B**). The
387 average SNAI1 activity of a heterogeneous population of *in silico* cells at increasing
388 ECM stiffness closely resembled its relative expression *in vitro* (**SM Fig. 5A**).

389 Additionally, the effect of matrix stiffness on migration was stronger under hypoxia,
390 aligning with the study's wound-healing results (**Fig. 4B**, *middle row*). Lastly, our
391 model predicts that matrix stiffness affects hypoxia-induced EMT more profoundly
392 than TGF-β induced EMT (**SM Fig. 5B**). The EMT-induction threshold of hypoxia is
393 increases rapidly on softer ECMs, while the effect on TGF-β-induced EMT is
394 significantly milder. We further predict that on soft ECMs that cannot support stress
395 fiber formation and migration, only a combination of strong hypoxia and near-
396 saturating TGF-β can induce EMT (**SM Fig. 5B**, *left*). In contrast, high cell density
397 blocks EMT in response to either signal as well as their combination, while isolated
398 mitogen-stimulated cells undergo biomechanically induced EMT even in the absence
399 of hypoxia or external TGF-β (**SM Fig. 5C**) (85).
400

401 **Figure 4. A stiff ECM aids hypoxia-induced EMT. A)** Dynamics of relevant
402 regulatory molecule expression in a quiescent cell on a soft ECM under hypoxia, in
403 response to increasing ECM stiffness (50 update-steps of 0, 25, 50, 75 and 100%
404 Stiff_ECM = ON at saturating mitogen exposure, moderate cell density and 5%
405 TGFb_secr knockdown). *X-axis:* update steps; *y-axis*: nodes organized by regulatory
406 module; *yellow/purple/blue scale*: 100% ON/ 50% on / 100% OFF; *black/white labels:*
407 relevant phenotypes; *update*: synchronous; *full time-course:* SM Fig. 4A. **B)** Fraction
408 of time normoxic (*left*) vs. hypoxic (*right*) cells at moderate density and saturating
409 mitogen exposure, plated on ECM of increasing stiffness, spend in: *top:* epithelial
410 (*yellow*), hybrid E/M (*dark yellow*) and mesenchymal (*mustard*) states; *middle*: non-
411 migrating (*light pink*), slow-migrating (*dark pink*) and fast-migrating (*brow-pink*)
412 states; *bottom:* quiescence (*orange*) vs. in cell cycle (*dark red*). *Length of time-window*
413 *for continuous runs:* 100 steps (~5 wild-type cell cycle lengths); *total sampled live cell*

414 *time:* 100,000 steps; *update*: synchronous; *initial condition for all sampling runs*:
415 epithelial cells in GF:1, CellDensity_Low:1, Stiff_ECM:1, Trail:0, Self_Loop:1,
416 TGFb_ext:0, Hypoxia:0; *environment of sampling runs:* Hypoxia:0(*left*)/1(*right*),
417 GF_High:1, CellDensity_Low:1; *autocrine TGF-β loop:* 95% (5% TGFb_secr
418 knockdown).

419

420 Loss of the Hif-1α repressor VHL aids metastatic cell
421 behaviors

422

423 Development of clear cell renal cell carcinoma (ccRCC) is marked by mutations
424 to Von Hippel Lindau gene, resulting in reduced expression or inactive forms of VHL
425 protein and aberrant Hif-1α expression under normoxia as well as hypoxia (106).
426 This mutation contributes to ccRCC being the 13th most common malignancy
427 throughout the world (107), as well as its reduced treatment efficacy and markedly
428 high mortality rate (108). While VHL loss is a hallmark of ccRCC, this mutation
429 alone is unable to consistently induce tumorigenesis in mice (109,110). Modeling
430 VHL deficient cells, we predict that the loss of VHL can drive metastatic cell
431 behaviors under biophysical microenvironments that do not induce EMT in wild-type
432 cells. To this end, we simulated wild type vs. 90% VHL knockdown in cells on soft
433 to stiff ECM, at densities ranging from isolated cells to dense fully confluent
434 monolayers under normoxia (**SM Fig. 6A**, *top left*). In the presence of a near-
435 saturating growth stimulus, only cells with some access spreading space and a very
436 stiff ECM underwent full EMT. In contrast, the combination of ECM and density

437 values leading to EMT were significantly expanded in VHL deficient cells. Loss of
438 VHL boosted full EMT rates particularly at moderate ECM stiffness, and in cells that
439 had only intermittent access to space to establish horizontal polarity (**SM Fig. 6A**,
440 *middle/bottom left*). While hypoxia blunted its effects, the boost to EMT was still
441 significant at moderate hypoxia (**SM Fig. 6A**, *middle/right columns*). As loss of VHL
442 stabilized Hif-1α, it also resulted in a full cell cycle arrest (**SM Fig. 6B**), indicating
443 that a boost to EMT in VHL-null cells would be counterbalanced by arrested growth.
444
445 Overall, our VHL-deficient simulations indicate that a combination of VHL loss
446 and cell cycle-promoting oncogene activation is required for cancer progression,
447 breaking Hif-1α and/or EMT-induced cell cycle arrest. Indeed, ccRCC tumors with a
448 VHL missense mutation often harbor Cdk4/6 and/or Cyclin D amplification and are
449 highly proliferative (111). Moreover, the most proliferative subtype of ccRCC is both
450 VHL deficient and have enhanced MYC activity (112). To test whether our model
451 could reprocure proliferation rescue in VHL-null cells, we re-ran the above
452 simulations at varying ECM stiffness and cell density in VHL-deficient cells with or
453 without Myc and/or Cyclin D hyper-activation (**SM Fig. 7A**). Intriguingly, only joint
454 hyper-activation of Myc and Cyclin D could significantly boost the proliferation of
455 VHL-deficient cells (**SM Fig. 7B***, left*). This co-occurred with a mild reduction in EMT
456 compared to VHL deficiency alone (**SM Fig. 7B***, right*). In contrast, pairing Cyclin D
457 with ccRCC-associated mutations upstream in the PI3K or MAPK pathway, such as
458 PI3K/mTORC1/ERK hyper-activation or p21/PTEN loss (113), only led to weak cell
459 cycle rescue (**SM Fig. 7C**; though most of these combinations also mildly boosted

460 EMT; not shown). Pairing Myc with the same cancer mutations only yielded weak
461 rescue with p21 loss, no cell cycle otherwise (**SM. Fig. D**).
462

463 Hypoxia prevents anoikis and epithelial apoptosis in
464 response to TGF-β

465

466 In addition to inducing a mesenchymal state, the lack of oxygen has been shown
467 to block anoikis and apoptosis; further contributing to the mortality rate of hypoxic
468 tumor formation (79,114). As previously shown in Sullivan et al.(85), our
469 mechanosensitive model can reproduce anoikis mediated epithelial cell death in
470 response to detachment from the extracellular matrix. To test if our model could
471 also replicate hypoxia-mediated evasion of anoikis, we simulated detachment of a
472 quiescent, isolated epithelial cell from a soft ECM exposed to saturating growth
473 factors (**Fig. 5A**; *full time-course:* **SM Fig. 8**). In contrast to normoxia, hypoxia
474 repressed pro-apoptotic factor activation and conferred anoikis resistance (76,115).
475 This was due to the ability of cells suspended under hypoxia to maintain high levels
476 of MAPK signaling and basal AKT activity. This was supported by hypoxia- and ROS-
477 mediated Src upregulation, an effect that did not require integrin-mediated
478 attachment and thus prevented anoikis (**Fig. 5A***, right*) (76). The non-canonical
479 hypoxic response also contributed anoikis resistance through NF-κB nuclear
480 translocation, reinforcing BCL-2 and BCL-X_L expression (116,117). Along similar
481 lines, our model reproduces TGF-β induced apoptosis of epithelial cells on a soft
482 matrix (**Fig. 5B***, left*) (118). Specifically, the model depicts an increase in BAX/BIM

483 signaling along with BCL-X_L loss, followed by apoptosis. In comparison, cells
484 exposed to TGF-β in a hypoxic environment are predicted to resist apoptosis
485 through increased Src and MAPK activity (**Fig. 5B***, right*).
486
487 **Figure 5. Hypoxia confers anoikis resistance and protection from TGF-β**
488 **induced epithelial cell apoptosis on a soft ECM. A)** Dynamics of relevant
489 regulatory molecule expression in a quiescent cell detached from a soft ECM in
490 normoxia (*left*) vs. hypoxia (*right*) (20 update-steps on soft ECM, 50 update-steps
491 detached, 100% high GF). **B)** Dynamics of relevant regulatory molecule expression in
492 a quiescent cell on a soft ECM, exposed to exogenous TGF-β in normoxia (*left*) vs.
493 hypoxia (*right*) (20 update-steps no TGF-β, 50 update-steps 100% TGF-β). *X-axis:*
494 update steps; *y-axis*: nodes organized by regulatory module; *yellow/blue*: ON/OFF;
495 *black/white labels:* relevant phenotypes; *update*: synchronous; *full time-course:* **SM**
496 **Fig. 8**.

497

498 Hypoxia and reoxygenation can drive the metastatic
499 cascade in the absence of exogenous transforming
500 signals

501

502 Next, we aimed to identify the biophysical microenvironments required for MET
503 following reoxygenation, a crucial step in the formation of secondary tumors (119).
504 To simulate a metastatic cascade, allowing for both intravasation and extravasation

505 from a solid tumor, we simulated a sequence of microenvironments designed to
506 mimic the signals metastatic cells experience en route from a solid tumor towards a
507 new metastatic site. To do this, we started with an epithelial cell at high cell density
508 on a stiff ECM, such as the basement membrane (120) (**Fig. 6A**, *pulse 1*). In a
509 growing solid tumor, this cell is likely to experience hypoxia (**Fig. 6A**, *pulse 2*). Yet,
510 due to density-dependent contact inhibition of proliferation as well as migration,
511 this epithelial cell requires the loss of neighbors (e.g., apoptosis of a neighbor) to
512 gain the room required for hypoxia-driven EMT (**Fig. 6A**, *pulse 3*). Migrating away
513 from the solid tumor, the cell can now reach areas of lower density and adequate
514 oxygen, while maintaining its mesenchymal state (**Fig. 6A**, *pulse 4*).
515
516 As hypoxia induces self-sustaining autocrine TGF-β signaling (14), transitioning
517 back to an epithelial state requires breaking the autocrine loop. This can happen
518 due to non-saturating TGF-β secretion in transit through the blood stream, where
519 cells have no access to a stiff ECM to keep mechanosensitive EMT signals active
520 (**Fig. 6A**, *pulse 5*). As a result, upon entering the vasculature, detachment from the
521 ECM and other cells is a crossroad with two phenotypic outcomes: cells that
522 maintain a mesenchymal state avoid anoikis, whereas cells that revert to an
523 epithelial state undergo apoptosis (**Fig. 6A**, *pulse 5*). Surviving cells then transition
524 to an epithelial state upon reaching high cell density in the new tissue (**Fig. 6A**,
525 *pulse 7*). From here, they can re-enter a proliferative hybrid E/M state once they
526 escape contact inhibition (121). This completes the metastatic cascade, leading to
527 new tumor growth. In contrast to cells with non-saturating autocrine TGF-β
528 signaling, saturating TGF-β secretion prevents apoptosis in nearly all cells

529 undergoing the metastatic cascade (**SM Fig. 9**). That said, even slight
530 perturbations of the autocrine loop, modeled by reducing *TGFb*_secr, are predicted
531 to have a major impact on the rate of apoptosis in the bloodstream, as well as upon
532 transitioning onto a soft ECM (**SM Fig. 10**).
533
534 **Figure 6. As cells follow the metastatic cascade, hypoxia-induced EMT**
535 **protects cells in circulation, reversed at the secondary site by high cell**
536 **density. A)** Dynamics of relevant regulatory molecule expression in an ensemble of
537 1000 quiescent epithelial cell exposed to a sequence of microenvironments along the
538 metastatic cascade (100 update-steps per pulse). *Pulse 1:* normoxia, stiff ECM, high
539 density; *Pulse 2:* hypoxia, stiff ECM, high density; *Pulse 3:* hypoxia, stiff ECM, medium
540 density; *Pulse 4* (invasion)*:* normoxia, stiff ECM, very low density; *Pulse 5*
541 (intravasation)*:* normoxia, no ECM, no neighbors; *Pulse 6* (extravasation)*:* normoxia,
542 soft ECM, low density; *Pulse 7* (MET)*:* normoxia, stiff ECM, high density; *X-axis:* update
543 steps; *y-axis*: nodes organized by regulatory module; *yellow/blue*: ON/OFF;
544 *black/white labels:* relevant phenotypes; *update*: synchronous; *autocrine TGF-β:* 5%
545 TGFb_secr knockdown; *full time-course:* **SM Fig. 8**. **B)** Average fraction of time an
546 ensemble of 1000 cells spend in *top:* non-migrating (*light pink*), slow-migrating (*dark*
547 *pink*) and fast-migrating (*brow-pink*) states; *middle*: epithelial (*yellow*), hybrid E/M
548 (*dark yellow*) and mesenchymal (*mustard*) states; *bottom:* survival (*red*) vs. in
549 apoptotic (*dark red*) states for each pulse along the metastatic cascade in panel A.
550
551 Another way to visualize the environment changes driving EMT and MET is to
552 highlight the cell state sequence the above steps push our model through, shown
553 on a comprehensive map of all relevant stable model phenotypes (attractors)

organized by microenvironment (**SM Figure 11**). Taken together, our mechanosensitive model can reproduce hypoxia-driven EMT, and its reversal based on a realistic sequence of its biophysical environments, depicting molecular signaling which occurs throughout the metastatic cascade.

Discussion

Despite the prevalence of hypoxic tumor microenvironments during solid tumor progression, the combined effect of hypoxia and the biophysical environment on cancer hallmarks remains underexplored. Here, we have built a dynamic regulatory network model focused on depicting the molecular signaling that occurs in response to oxygen deprivation (**Fig. 1**). To do this, we incorporated a hypoxic response module into our previously published mechanosensitive EMT model (85). Unlike published models exploring individual hypoxia-induced phenotypes (122–125), our model captures Hif-1α mediated transcription responsible for i) the induction as well as inhibition of proliferation (**Fig. 2**), ii) propelling EMT in a mechanosensitive manner (**Fig. 3-4**), and iii) preventing cell death in response to a changing TME (**Fig. 5**). Taken together, our model can reproduce cell state changes along a full metastatic cascade (**Fig. 6**), providing insight into the effects of a continuously changing biophysical environment during secondary tumor formation. The resulting cell behaviors cover cell-autonomous aspects of several cancer hallmarks, including *sustaining proliferative signaling*, *evading growth suppressors*, *activating invasion and metastasis*, *resisting cell death*, and *unlocking phenotypic plasticity* (126).

576

577 1. *Sustaining proliferative signaling & evading growth suppressors.* Our model
578 captures the paradoxical relationship between Hif-1α and proliferation. On
579 one hand, Hif-1α is required for proliferation through its role in upregulation
580 of the glycolytic machinery, including GLUT1, LDH-A, ALDA, and more
581 (modeled indirectly; **Fig. 2D**)(127). On the other hand, the increased
582 stability of Hif-1α under hypoxic conditions is known to induce cell cycle
583 arrest through functionally repressing Myc, a key driver of proliferation (**Fig.**
584 **2E**) (73,74). Indeed, our model predicts that Myc hyperactivation can rescue
585 the cell cycle under hypoxia (**SM Fig. 2**). In comparison to the effects of
586 *acute* oxygen deprivation captured by our model, *chronic* hypoxia increases
587 proliferation through Hif-2α-induced Myc transcription, increased MAPK/ERK
588 signaling, and YAP1 activation (128–130). Capturing this temporal shift in
589 our model is an area of future interest.

590

591 2. *Activating invasion and metastasis.* While the effects of hypoxia on EMT are
592 well-documented, the mechanosensitive nature of this response, as well as
593 its crosstalk with TGF-β signaling, have not been modeled individually or
594 collectively. Our model shows that hypoxia can induce EMT in cycling cells
595 (**Fig. 3**) (86), as long as they have access to a stiff ECM and some space to
596 spread (**Fig. 4**, **SM Fig 5**) (89). In contrast, normoxic cells only undergo
597 hybrid E/M in all but the most EMT-promoting biophysical environments (**SM**
598 **Fig. 5**). Once established, a mesenchymal state is maintained regardless of
599 hypoxia due to its ability to induce autocrine TGF-β signaling (**Fig. 3A**), even

600 in the presence of hyper-active VHL (100). Yet, this autocrine signal is not
601 required for EMT in hypoxic cells, as loss of TGF-β Receptor I does not block
602 the transition (**Fig. 3B**) (100). In contrast, TGF-β can only boost Hif-1α
603 stabilization in VHL-deficient cells. These nuances of crosstalk highlight the
604 importance of modeling the biophysical environments and genetic
605 interactions that compound the loss of VHL, a tumor suppressor pivotal to
606 clear cell renal cell carcinoma (ccRCC) tumorigenesis (108). These cancers
607 have among the highest rates of metastasis and mortality (131). Our model
608 predicts that VHL loss alone, known to predispose patients to cancer (132),
609 can push cells at moderate density and/or on a softer ECM into full EMT.
610 These cells undergo EMT instead of maintaining an epithelial state or a
611 reversible hybrid E/M phenotype required for repairing epithelial damage, as
612 expected in healthy cells (**SM Fig. 6**) (133). Furthermore, we highlight the
613 importance of secondary driver mutations that directly impact cell cycle
614 entry, such as joint cyclin D and Myc amplification / hyperactivation
615 (111,112). These mutations overcome the cell cycle arrest mediated by
616 hyperactive Hif-1α and/or autocrine TGF-β signaling (**SM Fig. 7**), helping
617 cancer cells combine sustained proliferation with an invasive mesenchymal
618 state.
619
620 *3.* *Resisting cell death.* Our model not only reproduces anoikis resistance of
621 epithelial cells under hypoxia (76), but also predicts that hypoxia can protect
622 epithelial cells on a soft ECM from TGF-β-induced apoptosis (**Fig. 5**).
623

624 4. *Unlocking phenotypic plasticity.* Our simulation of the metastatic cascade,
625 from hypoxia-induced EMT in a primary tumor through anoikis resistance in
626 the bloodstream to cell density-induced MET at a secondary site, our model
627 captures the non-genetic phenotypic plasticity cancer cells tap into as they
628 navigate different combinations of chemical and biomechanical environments
629 (**Fig. 6**). Interestingly, our model predicts that the ability to reach and
630 sustain a fully mesenchymal state, with no break in autocrine TGF-β
631 signaling, serves as an environmental bottleneck for circulating tumor cells
632 (**SM Fig. 9,10**). Moreover, intermittent (non-saturating) TGF-β signaling can
633 also render the transition back onto a soft ECM dangerous, as a weaker
634 mesenchymal program is less apt at warding off the apoptotic effects TGF-β
635 has on epithelial cells on soft ECM (85).
636
637 A particular strength of our model is its ability to reproduce a wide array of
638 experimental results in wild type, as well as mutant cells. Namely, the model
639 matched the direction and significance of molecular or phenotypic changed in 138
640 of 150 independently conduced experimental assays from 13 primary papers
641 focused on hypoxia and EMT (**SM Table 2**), and 7 of its 12 failures were due to
642 contradictory experiments included in our list. This validation lends weight to our
643 predictions, summarized below:
644 a) We predict that the loss of TGF-β signaling can weaken hypoxia-mediated cell
645 cycle arrest (**Fig. 3D**), and slow down hypoxia-induced EMT in cells with
646 weak mitogenic signaling (**SM Fig. 3**).

647 b) We predict that soft ECMs drastically raise the hypoxia threshold of EMT,
648 while they impact TGF-β more mildly. On very soft ECMs unable to support
649 stress fiber formation and migration, only a combination of strong hypoxia
650 and near-saturating TGF-β can induce EMT (**SM Fig. 5B**).
651 c) We predict that breaking the cell cycle inhibitory effects of VHL loss requires
652 combined hyper-activation of Myc *and* Cyclin D (**SM. Fig. 7**; less potent 2-
653 gene combinations involve either p21 loss or Cyclin D hyper-activation). In
654 contrast, upstream mutations that boost PI3K or MAPK signaling (alone or in
655 combination with Myc) cannot overcome cell cycle arrest mediated by Hif-1α
656 and/or TGF-β.
657 d) We predict that epithelial cells on a soft ECM exposed to TGF-β are protected
658 from apoptosis under hypoxic conditions (**Fig. 5B**).
659 e) Finally, we predict that circulating mesenchymal cells are highly sensitive to
660 intermittent weakening of autocrine TGF-β signaling, and thus only a fraction
661 of them survives anoikis (**SM. Fig. 9,10**). This could be tested with cell
662 suspension experiments on cells that first undergo EMT, treated with
663 increasing doses of TGF-β or TGF-β RI inhibitors.
664
665 Our use of a Boolean modeling framework, despite its advantages in allowing us to
666 build a 165-node regulatory network with 763 links, presents two technical
667 limitations of particular interest here (also discussed in (85)). *First,* modeling
668 autocrine signaling in a Boolean framework means that a positive feedback loop can
669 lock in between a signaling pathway and the transcription/secretion of the signal
670 itself, such as TGF-β. This loop implicitly assumes that a single mesenchymal cell

671 produces sufficient levels of bio-available TGF-β to maintain saturating signaling on
672 its own receptors; an assumption that is likely problematic. To get around the
673 resulting artifacts, we intentionally disrupted autocrine signaling using a 5%
674 reduction in secreted TGF-β in most of our simulations. This confers some
675 reversibility to EMT, permitting a fluid coexistence of mesenchymal and hybrid E/M
676 cells, the latter of which can divide. Yet, it is possible that *in vitro* the slow division
677 of mostly mesenchymal cells is not due to temporary loss of TGF-β signaling (as
678 modeled), but to the fact that even saturating levels of TGF-β do not fully block cell
679 cycle entry in mesenchymal cells.
680
681 A second technical limitation, detailed in (85), relates to our Boolean approximation
682 of ECM stiffness and cell density. There are three qualitatively distinct regimes for
683 these inputs: no ECM / soft ECM not capable of supporting stress fibers and growth
684 / stiff ECM that does. Similarly for density: no neighbors capable of making
685 junctions / some neighbors but also some space / full confluency with no room to
686 expand. Our Boolean model uses two linked nodes for each input, generating a 0 /
687 low / high state. This setup results in distinct signals in the 0 to low vs. the low to
688 high regimes, without overlap between them. This could result in more rigid model
689 responses near these boundaries than expected *in vitro.*
690
691 A different class of model limitations relates to the signaling biology we choose
692 to include or ignore. *First,* the five experiments our models failed to match that did
693 not contradict other data highlighted that at present our model is missing the
694 molecular mechanism responsible for Hif-1α-mediated G2 arrest (our model only

695 arrests in G1), as well as hypoxia-induced apoptosis (not modeled by choice).
696 *Second*, we restricted our focus to the *acute* hypoxic response governed primarily
697 by Hif-1α stabilization. Chronic hypoxia leads to a different set of responses our
698 model does not cover, as they are induced by Hif-2α stabilization (134). Despite
699 some conflicting data, it is generally accepted that the third HIF subunit, Hif-3α,
700 prevents Hif-1α transcriptional activity through sequestration of Hif-1β in a cell-type
701 specific manner (135,136). Expansion of the model to include these Hif-α subunits
702 are promising future directions required for modeling the temporal control of cell
703 fates under hypoxia.
704
705 *Third,* Hif-1α is a metabolic regulator, yet we only included its effects on energy
706 metabolism indirectly. The inclusion of a nutrient stimulus such as glucose, and the
707 energy sensing pathways that intersect with cell cycle entry modeled, in part, in
708 (137) would allow for a more precise accounting of the hypoxic response. For
709 example, apoptosis is differentially regulated based on nutrient loss in the presence
710 or absence of Hif-1α, as Hif-1α prevents metabolic stress-induced apoptosis (94).
711 Glucose transporters GLUT1/3 are also upregulated in mesenchymal cells,
712 demonstrating a shift towards glycolysis during EMT and suggesting a dependence
713 of EMT on nutrient levels for under hypoxia and/or normoxia (138). A future
714 expansion of our model could cover these responses, further mapping the
715 environment-combinations most conducive to EMT and MET.
716
717 *Fourth,* our model excludes several signaling pathways known to be differentially
718 regulated under hypoxia, such as Wnt, Sonic Hedgehog (Shh), Notch, Interleukin-6,

719 or TNF-α (139–146). Thus, we operate under the implicit assumption that these
720 signals are induced at equal levels in response to all stimuli tested within our model
721 – even though it is their regulation may also be mechanosensitive. These signals
722 are also implicated in mediating EMT, preventing apoptosis, and contributing to the
723 spatial and temporal regulation of EMT in response to a changing TME (147).
724 Overall, the integration of these pathways may offer further contextual insight into
725 cancer-associated behaviors increased by hypoxic tumor microenvironments.
726
727 Our model's replication of the metastatic cascade is a simplification of the highly
728 complex tumor and blood microenvironments experienced by circulating tumor
729 cells. Of note, extensive research has yielded both increasing and decreasing
730 metastatic potential through interactions with neutrophils, cancer associated
731 fibroblasts (CAFs), macrophages, platelets, and other cell types, all of which are
732 missing from our single-cell modeling approach (148–151). As an example,
733 interactions with platelets can upregulate TGF-β signaling and EMT, which help
734 prevent cell death during the circulating phase (152).
735
736 The model boundaries highlighted above stem, in part, from our single cell
737 approach. We find this single cell focus valuable for mapping the rules that govern
738 cell behavior in different microenvironments, a critical step towards building
739 multiscale models of cell communities and tissue architectures needed to approach
740 the complexity of tumor formation, tumor evolution and metastatic disease. Long-
741 term, our goal is two-fold. On the *single cell* modeling side, we plan to integrate the
742 model from this study with our Boolean model of mitochondrial dysfunction-

associated senescence, which shares this model's growth signaling / cell cycle and apoptosis modules (137). We will follow this with a detailed model of damage-induced cell cycle arrest mechanisms and a model of deep senescence, which can reverse mitochondrial dysfunction (153), but it is at least partially blocked in cells that underwent EMT (154,155). The resulting single-cell model would be able to address most cell-autonomous cancer hallmarks. On the *tissue* modeling side, the above single-cell model can serve as the engine inside agents of multicellular, spatial model of epithelial homeostasis and carcinoma development.

Computational Methods

I. Boolean model building. To build our model we extended our previously published mechanosensitive EMT model (85) with a hypoxia-sensing signaling module. The model synthesizes experimental data from 540 papers into a 165-node Boolean network with 763 regulatory links. All links and regulatory functions are experimentally justified in **SM Table 1**. Our model construction approach, the rationale for using synchronous update, storing our model in *Dynamically Modular Model Specification* (.*dmms*) format are detailed in the *Supplementary Methods* of (137) and STAR Methods of (85). All model files and other files required to run the model and reproduce all results, are packaged into **SM Files 1-3**.

II. Model availability. Model files in *SBML* format (used by BioModels (156), *GinSim* (157) and *The Cell Collective* (158)), *dmms* format (used by our discrete-state modeling software *dynmod*), *BooleanNet* format (used by the BooleanNet

765 Python library (159)), and an editable network visualization in *graphml* format (read
766 by yED (160)) are included in **SM Files 1**.

767 ***III.* Dynmod *Boolean modeling software.*** Boolean simulations and analysis were
768 performed with the discrete-state modeling software *dynmod* (137), available on
769 GitHub at *https://github.com/Ravasz-Regan-Group/dynmod* (our justification for
770 using in-house software, along with instructions to install Haskell and compile
771 *dynmod* are detailed in the *Suppl. Methods* of (137)). Briefly, our code can: **a)**
772 automatically map each attractor to a combinatorial phenotype profile (e.g.,
773 quiescent, alive, MiDAS) based on user-defined signatures attached to regulatory
774 switches; **b)** visualize and filter attractors of interest via their phenotype profiles,
775 organizing them within a coordinate system of independent environmental input-
776 combinations; **c)** set up simulations by specifying the initial environment and
777 phenotypic state of the cell, rather than each node state; **d)** collect phenotype
778 statistics on large ensembles of non-interacting cells (independent simulation runs)
779 in non-saturating environments and/or non-saturating perturbations (e.g., 10%
780 Hypoxia, 50% VHL inhibition); **e)** generate simulation-series that explore the model's
781 behavior across a range of environmental inputs, combinations of 2-3 inputs, and/or
782 the effects of increasing node knockdown / hyper-activation (alone or in combination
783 with changing environmental input levels; with/without additional background
784 mutations); and **f)** use metadata from *dmms* files to generate a formatted table with
785 all biological documentation (**SM Table 1**).
786

787 To run simulations (including attractor sampling), *dynmod* parses user-generated
788 experiment files (*.vex* format). The **SM File 1** package includes two *.vex* our readers

can use to reproduce all simulations used in our figures (*Hypoxia_EMT_Main_Fig.vex, Hypoxia_EMT_SM_Fig.vex*). Similarly, the **SM File 2** package contains the isolated EMT module model (*EMT_Module_Hypoxia.dmms*), the *EMT_Module.vex* file, and time courses that showcase the model attractors visualized on **Fig. 1B**. Finally, **SM File 3** contains the *.vex* file and script required for rerunning our validation experiments (see below). Additional information to run the simulations is available upon request from E.R.R.

IV. Attractor detection with* dynmod*. *Dynmod* uses synchronous update to find stable phenotypes and/or oscillations (attractors) via a stochastic sampling procedure (161) detailed in (162–164,85). Briefly, we typically find attractors by running noisy time-courses of length *T=25* with noise *p=0.02* from *N=100* different random initial conditions for each unique combination of environmental inputs (N_{total} = 100*2^7 = 128,000 random initial conditions). For each observed state along these time-courses, the synchronous attractor basin is determined, recorded, and exported as a *.csv* file (*Greene_Hypoxia_Model_attractors_a100_25_2.0e-2.csv* in the **SM File 1** package). To re-sample the model's attractors, edit the *Sampling*{…} command block near the top of *Hypoxia_EMT_Main_Fig.vex* to switch from the currently active *Read:* directive to the commented-out *Sample:* line.

V. Running simulations with* dynmod*. Precise use of each command is described in *Hypoxia_EMT_Main_Fig.vex* and *Hypoxia_EMT_SM_Fig.vex* (in **SM File 1**), which are executed by *dynmod* using the **-e** command-line tag:

```
dynmod Hypoxia_EMT_Model.dmms -e Hypoxia_EMT_Main_Fig.vex
```

```
dynmod Hypoxia_EMT_Model.dmms -e Hypoxia_EMT_SM_Fig.vex
```

These files include instructions to simulate and visualize: **a)** synchronous time courses from a subset of cell states in a given initial environment, exposed to reversible changes in a single environmental signal (e.g., **Fig. 2A**); **b)** non-saturating environments where an input is stochastically tuned between 0 and 1 (e.g., **Fig. 4A**); **c)** partial or full knockdown/hyper-activation of arbitrary sets of nodes (e.g., **Fig. 3**; justification and limitations in (85)); **d)** combine these in an arbitrary sequence of perturbations and environments defined in distinct time windows (e.g., **Fig. 6**); **e)** average activity of all nodes and/or all module phenotypes in an ensemble of independent cells (e.g., **Fig. 2B**); **f)** bar charts of the activity of user-specified nodes and/or module phenotypes, averaged over an ensemble of independent runs and across each distinct time window of an experiment (e.g., **SM Fig. 3**); **g)** bar charts and heatmaps showing the model's behavior (module phenotype states) across a range of environments and/or node perturbations (e.g., **SM Fig. 6**).

VI. Model validation. To test the model's ability to reproduce experimentally observed cell behaviors and/or molecular changes related to EMT in general and hypoxic responses on particular, we curated a list of 150 distinct observations from 13 relevant primary articles (**SM Table 2**). These observations cover knockdown or overexpression of 19 different proteins or microRNAs. For each *in vitro* experiment, we created matching *in silico* experiments or experiment-pairs that mimicked the extracellular environment and perturbations such as knockdowns or overexpression. This extensive validation protocol is included in *Hypoxia_EMT_Validation.vex* (in **SM File 3**). Running

```
dynmod Hypoxia_EMT_Model.dmms -e Hypoxia_EMT_ Validation.vex
```

generates simulation data on a population of cells for each experimental condition. To automate the 229 comparisons, each *in vitro* observation in **SM Table 2** is accompanied by information about the name and location of its matching *in silico* data (experiment names, relevant time windows, code pointing to the correct attractor file). The Python script *Hypoxia Model Validation Script.py* reads a *.csv* version of **SM Table 2**, as well as the simulation data, to perform unpaired t-tests, list, save and summarize the validation results as the percentage of observations our model can reproduce (script and *.csv* in **SM File 3**). Simulation results are considered a match for the experiment if either of the following conditions are met: *i)* there is a significant change in the same direction as the *in vitro* result, and the change is at least 5% of the average of the two values compared, or *ii)* no change, no significant change, or smaller than 5% difference, matching an *in vitro* result showing no significant change. The script also generates figures for each comparison (**SM File 4**); the 17 failed comparisons identified by the script were manually marked with red/orange "*Mismatch*" labels (*red*: model does not match biological outcome; *orange*: different experiments give conflicting results; model matches other outcome).

VII. Metadata table, 2D network visualization and model conversion.

a) To generate a formatted table with all model metadata included in the `.dmms` file, run `dynmod Hypoxia_EMT_Model.dmms -w -s`

This generates a text file with metadata warning (e.g., missing descriptions, citations, unrecognized node/link types), and a folder containing the LaTeX and BibTeX reference files used to render **SM Table 1**. To generate the pdf, use LaTeX or *https://www.overleaf.com*.

b) To generate a `.gml` file read by the network visualization software yED run

```
dynmod Hypoxia_EMT_Model.dmms -g
```

The resulting visualization can be modified in yED to alter node coordinates and node colors. As long as none of the links or groupings are altered in the editing process, and the changes are saved in `.gml` format, running

```
dynmod Hypoxia_EMT_Model.dmms -u Hypoxia_EMT_Model.gml
```

will read the altered coordinates and colors, then generate an updated `.dmms` file (with a new name). **Fig. 1** was generated in yED by manual post-professing of the auto generated `.gml` file (i.e., removal of groups, altered label colors for better contrast, creation of sub-networks).

c) To generate a `.BooleanNet` version of the model, run

```
dynmod Hypoxia_EMT_Model.dmms -t
```

d) To generate the `.sbml` version, use *bioLQM* (http://colomoto.org/biolqm/) with the command:

```
java -jar bioLQM-0.8-SNAPSHOT.jar Hypoxia_EMT_Model_Fine.booleannet
Hypoxia_EMT_Model.sbml
```

VIII. Previously introduced regulatory modules. Detailed descriptions of *Growth factor signaling*, *Replication origin licensing*, *Restriction switch*, *Mitotic phase switch*, *Apoptotic switch*, *Cell cycle processes, Adhesion, Contact Inhibition, EMT* and *TGF-β signaling* are detailed in (85).

Acknowledgments

We thank Peter L. Regan for the ongoing improvement of the *dynmod* software package used to generate all modeling results. All funding for this study was provided by The College of Wooster. E.R. would like to thank the Henry Luce III Fund for Distinguished Scholarship, the Faculty Development Funds and the Life Sciences Endowed Funds for research support. I.Z thanks the Henry J. Copeland Independent Study Fund for research travel support. G.G. thanks the Biochemistry and Molecular Biology Program for support to present his work.

Author Contributions

G.G. - conceptualization, data curation, formal analysis, investigation, validation, visualization, writing - original draft, writing – review & editing (built hypoxia signaling modules, Boolean model development, ran simulations, designed validation, generated predictions, figures, wrote first draft of the manuscript).

I.Z. - conceptualization, data curation, formal analysis, investigation (built hypoxia signaling modules, Boolean model development, ran simulations).

E.R.R - conceptualization, data curation, formal analysis, funding acquisition, investigation, methodology, project administration, supervision, validation, visualization, writing - original draft, writing – review & editing (supervised project,

built hypoxia signaling modules, guided Boolean modeling software development, developed simulation methods, ran simulations, designed validation, generated predictions, figures, edited and finalized manuscript).

References

1. de Visser KE, Joyce JA. The evolving tumor microenvironment: From cancer initiation to metastatic outgrowth. Cancer Cell. 2023 Mar 13;41(3):374–403.

2. Anderson NM, Simon MC. The tumor microenvironment. Current Biology. 2020 Aug 17;30(16):R921–5.

3. Cacho-Díaz B, García-Botello DR, Wegman-Ostrosky T, Reyes-Soto G, Ortiz-Sánchez E, Herrera-Montalvo LA. Tumor microenvironment differences between primary tumor and brain metastases. J Transl Med. 2020 Jan 3;18(1):1.

4. Zeppellini A, Galimberti S, Leone BE, Pacifico C, Riva F, Cicchiello F, et al. Comparison of tumor microenvironment in primary and paired metastatic ER+/HER2- breast cancers: results of a pilot study. BMC Cancer. 2021 Mar 10;21(1):260.

5. Kim R, Keam B, Kim S, Kim M, Kim SH, Kim JW, et al. Differences in tumor microenvironments between primary lung tumors and brain metastases in lung cancer patients: therapeutic implications for immune checkpoint inhibitors. BMC Cancer. 2019 Jan 7;19(1):19.

6. Neophytou CM, Panagi M, Stylianopoulos T, Papageorgis P. The Role of Tumor Microenvironment in Cancer Metastasis: Molecular Mechanisms and Therapeutic Opportunities. Cancers (Basel). 2021 Apr 23;13(9):2053.

7. Dillekås H, Rogers MS, Straume O. Are 90% of deaths from cancer caused by metastases? Cancer Med. 2019 Aug 8;8(12):5574–6.

8. Son H, Moon A. Epithelial-mesenchymal Transition and Cell Invasion. Toxicol Res. 2010 Dec;26(4):245–52.

9. Dongre A, Weinberg RA. New insights into the mechanisms of epithelial–mesenchymal transition and implications for cancer. Nat Rev Mol Cell Biol. 2019 Feb;20(2):69–84.

10. Dudás J, Ladányi A, Ingruber J, Steinbichler TB, Riechelmann H. Epithelial to Mesenchymal Transition: A Mechanism that Fuels Cancer Radio/Chemoresistance. Cells. 2020 Feb 12;9(2):428.

932 11. Lu M, Jolly MK, Levine H, Onuchic JN, Ben-Jacob E. MicroRNA-based regulation
933 of epithelial–hybrid–mesenchymal fate determination. Proc Natl Acad Sci USA.
934 2013 Nov 5;110(45):18144–9.

935 12. Tian XJ, Zhang H, Xing J. Coupled Reversible and Irreversible Bistable Switches
936 Underlying TGFβ-induced Epithelial to Mesenchymal Transition. Biophysical
937 Journal. 2013 Aug;105(4):1079–89.

938 13. Siemens H, Jackstadt R, Hünten S, Kaller M, Menssen A, Götz U, et al. miR-34
939 and SNAIL form a double-negative feedback loop to regulate epithelial-
940 mesenchymal transitions. Cell Cycle. 2011 Dec 15;10(24):4256–71.

941 14. Gregory PA, Bracken CP, Smith E, Bert AG, Wright JA, Roslan S, et al. An
942 autocrine TGF-beta/ZEB/miR-200 signaling network regulates establishment
943 and maintenance of epithelial-mesenchymal transition. Mol Biol Cell. 2011 May
944 15;22(10):1686–98.

945 15. Zhang J, Tian XJ, Zhang H, Teng Y, Li R, Bai F, et al. TGF-β-induced epithelial-
946 to-mesenchymal transition proceeds through stepwise activation of multiple
947 feedback loops. Science Signaling. 2014 Sep;7(345):ra91.

948 16. Grosse-Wilde A, Fouquier d'Hérouël A, McIntosh E, Ertaylan G, Skupin A,
949 Kuestner RE, et al. Stemness of the hybrid Epithelial/Mesenchymal State in
950 Breast Cancer and Its Association with Poor Survival. PLoS One.
951 2015;10(5):e0126522.

952 17. Huang RYJ, Wong MK, Tan TZ, Kuay KT, Ng AHC, Chung VY, et al. An EMT
953 spectrum defines an anoikis-resistant and spheroidogenic intermediate
954 mesenchymal state that is sensitive to e-cadherin restoration by a src-kinase
955 inhibitor, saracatinib (AZD0530). Cell Death Dis. 2013 Nov 7;4:e915.

956 18. Jolly MK, Tripathi SC, Jia D, Mooney SM, Celiktas M, Hanash SM, et al. Stability
957 of the hybrid epithelial/mesenchymal phenotype. Oncotarget. 2016 Mar
958 17;7(19):27067–84.

959 19. Dong J, Hu Y, Fan X, Wu X, Mao Y, Hu B, et al. Single-cell RNA-seq analysis
960 unveils a prevalent epithelial/mesenchymal hybrid state during mouse
961 organogenesis. Genome Biol. 2018 Mar 14;19(1):31.

962 20. Gonzalez VD, Samusik N, Chen TJ, Savig ES, Aghaeepour N, Quigley DA, et al.
963 Commonly Occurring Cell Subsets in High-Grade Serous Ovarian Tumors
964 Identified by Single-Cell Mass Cytometry. Cell Rep. 2018 Feb 13;22(7):1875–
965 88.

966 21. Karacosta LG, Anchang B, Ignatiadis N, Kimmey SC, Benson JA, Shrager JB, et
967 al. Mapping lung cancer epithelial-mesenchymal transition states and
968 trajectories with single-cell resolution. Nat Commun. 2019 Dec 6;10(1):5587.

969 22. Puram SV, Tirosh I, Parikh AS, Patel AP, Yizhak K, Gillespie S, et al. Single-cell
970 transcriptomic analysis of primary and metastatic tumor ecosystems in head
971 and neck cancer. Cell. 2017 Dec 14;171(7):1611-1624.e24.

972 23. Biswas K, Jolly MK, Ghosh A. Stability and mean residence times for hybrid
973 epithelial/mesenchymal phenotype. Phys Biol. 2019 Jan 29;16(2):025003.

974 24. Hong T, Watanabe K, Ta CH, Villarreal-Ponce A, Nie Q, Dai X. An Ovol2-Zeb1
975 Mutual Inhibitory Circuit Governs Bidirectional and Multi-step Transition
976 between Epithelial and Mesenchymal States. PLoS Comput Biol. 2015 Nov
977 10;11(11):e1004569.

978 25. Bocci F, Gearhart-Serna L, Boareto M, Ribeiro M, Ben-Jacob E, Devi GR, et al.
979 Toward understanding cancer stem cell heterogeneity in the tumor
980 microenvironment. Proc Natl Acad Sci U S A. 2019 Jan 2;116(1):148–57.

981 26. Tripathi S, Chakraborty P, Levine H, Jolly MK. A mechanism for epithelial-
982 mesenchymal heterogeneity in a population of cancer cells. PLoS Comput Biol.
983 2020 Feb;16(2):e1007619.

984 27. Steinway SN, Zañudo JGT, Ding W, Rountree CB, Feith DJ, Loughran TP, et al.
985 Network modeling of TGFβ signaling in hepatocellular carcinoma epithelial-to-
986 mesenchymal transition reveals joint sonic hedgehog and Wnt pathway
987 activation. Cancer Research. 2014 Nov;74(21):5963–77.

988 28. Gómez Tejeda Zañudo J, Guinn MT, Farquhar K, Szenk M, Steinway SN, Balázsi
989 G, et al. Towards control of cellular decision-making networks in the epithelial-
990 to-mesenchymal transition. Phys Biol. 2019 07;16(3):031002.

991 29. Steinway SN, Zañudo JGT, Michel PJ, Feith DJ, Loughran TP, Albert R.
992 Combinatorial interventions inhibit TGFβ-driven epithelial-to-mesenchymal
993 transition and support hybrid cellular phenotypes. NPJ systems biology and
994 applications. 2015;1:15014.

995 30. Li Y, Zhao L, Li XF. Hypoxia and the Tumor Microenvironment. Technol Cancer
996 Res Treat. 2021 Aug 5;20:15330338211036304.

997 31. Jiang BH, Semenza GL, Bauer C, Marti HH. Hypoxia-inducible factor 1 levels
998 vary exponentially over a physiologically relevant range of O2 tension.
999 American Journal of Physiology-Cell Physiology. 1996 Oct;271(4):C1172–80.

1000 32. Krock BL, Skuli N, Simon MC. Hypoxia-Induced Angiogenesis. Genes Cancer.
1001 2011 Dec;2(12):1117–33.

1002 33. Saxena K, Jolly MK, Balamurugan K. Hypoxia, partial EMT and collective
1003 migration: Emerging culprits in metastasis. Transl Oncol. 2020 Aug
1004 8;13(11):100845.

1005 34. Jeltsch M, Leppänen VM, Saharinen P, Alitalo K. Receptor Tyrosine Kinase-
1006 Mediated Angiogenesis. Cold Spring Harb Perspect Biol. 2013
1007 Sep;5(9):a009183.

1008 35. Jiang X, Wang J, Deng X, Xiong F, Zhang S, Gong Z, et al. The role of
1009 microenvironment in tumor angiogenesis. Journal of Experimental & Clinical
1010 Cancer Research. 2020 Sep 30;39(1):204.

1011 36. Cichon MA, Nelson CM, Radisky DC. Regulation of Epithelial-Mesenchymal
1012 Transition in Breast Cancer Cells by Cell Contact and Adhesion. Cancer Inform.
1013 2015 Feb 9;14(Suppl 3):1–13.

1014 37. O'Connor JW, Mistry K, Detweiler D, Wang C, Gomez EW. Cell-cell contact and
1015 matrix adhesion promote αSMA expression during TGFβ1-induced epithelial-
1016 myofibroblast transition via Notch and MRTF-A. Sci Rep. 2016 May
1017 19;6(1):26226.

1018 38. Rice AJ, Cortes E, Lachowski D, Cheung BCH, Karim SA, Morton JP, et al.
1019 Matrix stiffness induces epithelial-mesenchymal transition and promotes
1020 chemoresistance in pancreatic cancer cells. Oncogenesis. 2017 Jul
1021 3;6(7):e352.

1022 39. Tian H, Shi H, Yu J, Ge S, Ruan J. Biophysics Role and Biomimetic Culture
1023 Systems of ECM Stiffness in Cancer EMT. Glob Chall. 2022 Mar
1024 20;6(6):2100094.

1025 40. Aldea M, Andre F, Marabelle A, Dogan S, Barlesi F, Soria JC. Overcoming
1026 Resistance to Tumor-Targeted and Immune-Targeted Therapies. Cancer
1027 Discovery. 2021 Apr 1;11(4):874–99.

1028 41. Taeb S, Ashrafizadeh M, Zarrabi A, Rezapoor S, Musa AE, Farhood B, et al.
1029 Role of Tumor Microenvironment in Cancer Stem Cells Resistance to
1030 Radiotherapy. Current Cancer Drug Targets. 2022 Jan 1;22(1):18–30.

1031 42. Zhao D, Mo Y, Neganova ME, Aleksandrova Y, Tse E, Chubarev VN, et al. Dual
1032 effects of radiotherapy on tumor microenvironment and its contribution
1033 towards the development of resistance to immunotherapy in gastrointestinal
1034 and thoracic cancers. Front Cell Dev Biol. 2023 Oct 3;11:1266537.

1035 43. Luqmani YA. Mechanisms of Drug Resistance in Cancer Chemotherapy. Medical
1036 Principles and Practice. 2008 Jul 9;14(Suppl. 1):35–48.

1037 44. Fletcher NM, Belotte J, Saed MG, Memaj I, Diamond MP, Morris RT, et al.
1038 Specific point mutations in key redox enzymes are associated with
1039 chemoresistance in epithelial ovarian cancer. Free Radic Biol Med. 2017
1040 Jan;102:122–32.

1041 45. Appelhoff RJ, Tian YM, Raval RR, Turley H, Harris AL, Pugh CW, et al.
1042 Differential Function of the Prolyl Hydroxylases PHD1, PHD2, and PHD3 in the

1043 Regulation of Hypoxia-inducible Factor *. Journal of Biological Chemistry. 2004
1044 Sep 10;279(37):38458–65.

1045 46. Peng J, Wang X, Ran L, Song J, Luo R, Wang Y. Hypoxia-Inducible Factor 1α
1046 Regulates the Transforming Growth Factor β1/SMAD Family Member 3 Pathway
1047 to Promote Breast Cancer Progression. J Breast Cancer. 2018 Sep;21(3):259–
1048 66.

1049 47. Ananth S, Knebelmann B, Grüning W, Dhanabal M, Walz G, Stillman IE, et al.
1050 Transforming growth factor beta1 is a target for the von Hippel-Lindau tumor
1051 suppressor and a critical growth factor for clear cell renal carcinoma. Cancer
1052 Res. 1999 May 1;59(9):2210–6.

1053 48. Fong GH, Takeda K. Role and regulation of prolyl hydroxylase domain proteins.
1054 Cell Death Differ. 2008 Apr;15(4):635–41.

1055 49. Kamura T, Sato S, Iwai K, Czyzyk-Krzeska M, Conaway RC, Conaway JW.
1056 Activation of HIF1α ubiquitination by a reconstituted von Hippel-Lindau (VHL)
1057 tumor suppressor complex. Proc Natl Acad Sci U S A. 2000 Sep
1058 12;97(19):10430–5.

1059 50. Lando D, Peet DJ, Gorman JJ, Whelan DA, Whitelaw ML, Bruick RK. FIH-1 is an
1060 asparaginyl hydroxylase enzyme that regulates the transcriptional activity of
1061 hypoxia-inducible factor. Genes Dev. 2002 Jun 15;16(12):1466–71.

1062 51. Prabhakar NR, Semenza GL. ADAPTIVE AND MALADAPTIVE
1063 CARDIORESPIRATORY RESPONSES TO CONTINUOUS AND INTERMITTENT
1064 HYPOXIA MEDIATED BY HYPOXIA-INDUCIBLE FACTORS 1 AND 2. Physiol Rev.
1065 2012 Jul;92(3):967–1003.

1066 52. Semenza GL. HIF-1 and mechanisms of hypoxia sensing. Current Opinion in
1067 Cell Biology. 2001 Apr 1;13(2):167–71.

1068 53. Prabhakar NR, Semenza GL. Adaptive and Maladaptive Cardiorespiratory
1069 Responses to Continuous and Intermittent Hypoxia Mediated by Hypoxia-
1070 Inducible Factors 1 and 2. Physiological Reviews. 2012 Jul;92(3):967–1003.

1071 54. Koh MY, Lemos R, Liu X, Powis G. The Hypoxia-Associated Factor Switches
1072 Cells from HIF-1α– to HIF-2α–Dependent Signaling Promoting Stem Cell
1073 Characteristics, Aggressive Tumor Growth and Invasion. Cancer Res. 2011 Jun
1074 1;71(11):4015–27.

1075 55. Makino Y, Uenishi R, Okamoto K, Isoe T, Hosono O, Tanaka H, et al.
1076 Transcriptional Up-regulation of Inhibitory PAS Domain Protein Gene
1077 Expression by Hypoxia-inducible Factor 1 (HIF-1): A NEGATIVE FEEDBACK
1078 REGULATORY CIRCUIT IN HIF-1-MEDIATED SIGNALING IN HYPOXIC CELLS.
1079 Journal of Biological Chemistry. 2007 May 11;282(19):14073–82.

1080 56. Duan C. Hypoxia-inducible factor 3 biology: complexities and emerging
1081 themes. Am J Physiol Cell Physiol. 2016 Feb 15;310(4):C260-269.

1082 57. Li QF, Wang XR, Yang YW, Lin H. Hypoxia upregulates hypoxia inducible factor
1083 (HIF)-3α expression in lung epithelial cells: characterization and comparison
1084 with HIF-1α. Cell Res. 2006 Jun;16(6):548–58.

1085 58. Main AM, Gillberg L, Jacobsen AL, Nilsson E, Gjesing AP, Hansen T, et al. DNA
1086 methylation and gene expression of HIF3A: cross-tissue validation and
1087 associations with BMI and insulin resistance. Clin Epigenetics. 2016 Sep
1088 2;8(1):89.

1089 59. Benita Y, Kikuchi H, Smith AD, Zhang MQ, Chung DC, Xavier RJ. An integrative
1090 genomics approach identifies Hypoxia Inducible Factor-1 (HIF-1)-target genes
1091 that form the core response to hypoxia. Nucleic Acids Res. 2009
1092 Aug;37(14):4587–602.

1093 60. Wang V, Davis DA, Haque M, Huang LE, Yarchoan R. Differential Gene Up-
1094 Regulation by Hypoxia-Inducible Factor-1α and Hypoxia-Inducible Factor-2α in
1095 HEK293T Cells. Cancer Research. 2005 Apr 15;65(8):3299–306.

1096 61. Manalo DJ, Rowan A, Lavoie T, Natarajan L, Kelly BD, Ye SQ, et al.
1097 Transcriptional regulation of vascular endothelial cell responses to hypoxia by
1098 HIF-1. Blood. 2005 Jan 15;105(2):659–69.

1099 62. Zhang L, Huang G, Li X, Zhang Y, Jiang Y, Shen J, et al. Hypoxia induces
1100 epithelial-mesenchymal transition via activation of SNAI1 by hypoxia-inducible
1101 factor -1α in hepatocellular carcinoma. BMC Cancer. 2013 Mar 9;13:108.

1102 63. Zhang W, Shi X, Peng Y, Wu M, Zhang P, Xie R, et al. HIF-1α Promotes
1103 Epithelial-Mesenchymal Transition and Metastasis through Direct Regulation of
1104 ZEB1 in Colorectal Cancer. PLOS ONE. 2015 Jun 9;10(6):e0129603.

1105 64. Schödel J, Oikonomopoulos S, Ragoussis J, Pugh CW, Ratcliffe PJ, Mole DR.
1106 High-resolution genome-wide mapping of HIF-binding sites by ChIP-seq. Blood.
1107 2011 Jun 9;117(23):e207–17.

1108 65. Morikawa M, Koinuma D, Miyazono K, Heldin CH. Genome-wide mechanisms of
1109 Smad binding. Oncogene. 2013 Mar;32(13):1609–15.

1110 66. Mallikarjuna P, Sitaram RT, Landström M, Ljungberg B. VHL status regulates
1111 transforming growth factor-β signaling pathways in renal cell carcinoma.
1112 Oncotarget. 2018 Mar 27;9(23):16297–310.

1113 67. Dai Y, Siemann D. c-Src is required for hypoxia-induced metastasis-associated
1114 functions in prostate cancer cells. Onco Targets Ther. 2019 May 8;12:3519–29.

1115 68. Guo Q, Lu L, Liao Y, Wang X, Zhang Y, Liu Y, et al. Influence of c-Src on
1116 hypoxic resistance to paclitaxel in human ovarian cancer cells and reversal of
1117 FV-429. Cell Death Dis. 2018 Jan;8(1):e3178–e3178.

1118 69. Lee G, Won HS, Lee YM, Choi JW, Oh TI, Jang JH, et al. Oxidative Dimerization
1119 of PHD2 is Responsible for its Inactivation and Contributes to Metabolic
1120 Reprogramming via HIF-1α Activation. Sci Rep. 2016 Jan 7;6(1):18928.

1121 70. Hu X, Wu X, Xu J, Zhou J, Han X, Guo J. Src kinase up-regulates the ERK
1122 cascade through inactivation of protein phosphatase 2A following cerebral
1123 ischemia. BMC Neurosci. 2009 Jul 14;10:74.

1124 71. Owens DW, McLean GW, Wyke AW, Paraskeva C, Parkinson EK, Frame MC, et
1125 al. The Catalytic Activity of the Src Family Kinases Is Required to Disrupt
1126 Cadherin-dependent Cell–Cell Contacts. MBoC. 2000 Jan;11(1):51–64.

1127 72. Zhang X, Guo J, Jabbarzadeh Kaboli P, Zhao Q, Xiang S, Shen J, et al. Analysis
1128 of Key Genes Regulating the Warburg Effect in Patients with Gastrointestinal
1129 Cancers and Selective Inhibition of This Metabolic Pathway in Liver Cancer
1130 Cells. Onco Targets Ther. 2020 Jul 27;13:7295–304.

1131 73. Goda N, Ryan HE, Khadivi B, McNulty W, Rickert RC, Johnson RS. Hypoxia-
1132 Inducible Factor 1α Is Essential for Cell Cycle Arrest during Hypoxia. Mol Cell
1133 Biol. 2003 Jan;23(1):359–69.

1134 74. Koshiji M, Kageyama Y, Pete EA, Horikawa I, Barrett JC, Huang LE. HIF-1α
1135 induces cell cycle arrest by functionally counteracting Myc. EMBO J. 2004 May
1136 5;23(9):1949–56.

1137 75. Chen Y, Yan H, Yan L, Wang X, Che X, Hou K, et al. Hypoxia-induced ALDH3A1
1138 promotes the proliferation of non-small-cell lung cancer by regulating energy
1139 metabolism reprogramming. Cell Death Dis. 2023 Sep 20;14(9):1–11.

1140 76. Whelan KA, Caldwell SA, Shahriari KS, Jackson SR, Franchetti LD, Johannes GJ,
1141 et al. Hypoxia Suppression of Bim and Bmf Blocks Anoikis and Luminal Clearing
1142 during Mammary Morphogenesis. Mol Biol Cell. 2010 Nov 15;21(22):3829–37.

1143 77. Rohwer N, Welzel M, Daskalow K, Pfander D, Wiedenmann B, Detjen K, et al.
1144 Hypoxia-Inducible Factor 1α Mediates Anoikis Resistance via Suppression of α5
1145 Integrin. Cancer Research. 2008 Dec 15;68(24):10113–20.

1146 78. Saikumar P, Dong Z, Patel Y, Hall K, Hopfer U, Weinberg JM, et al. Role of
1147 hypoxia-induced Bax translocation and cytochrome c release in reoxygenation
1148 injury. Oncogene. 1998 Dec;17(26):3401–15.

1149 79. Greijer AE, van der Wall E. The role of hypoxia inducible factor 1 (HIF-1) in
1150 hypoxia induced apoptosis. J Clin Pathol. 2004 Oct;57(10):1009–14.

1151 80. Dong Z, Venkatachalam MA, Wang J, Patel Y, Saikumar P, Semenza GL, et al.
1152 Up-regulation of apoptosis inhibitory protein IAP-2 by hypoxia. Hif-1-
1153 independent mechanisms. J Biol Chem. 2001 Jun 1;276(22):18702–9.

1154 81. Dagogo-Jack I, Shaw AT. Tumour heterogeneity and resistance to cancer
1155 therapies. Nat Rev Clin Oncol. 2018 Feb;15(2):81–94.

1156 82. Jacquemin V, Antoine M, Dom G, Detours V, Maenhaut C, Dumont JE. Dynamic
1157 Cancer Cell Heterogeneity: Diagnostic and Therapeutic Implications. Cancers
1158 (Basel). 2022 Jan 7;14(2):280.

1159 83. Simeonov KP, Byrns CN, Clark ML, Norgard RJ, Martin B, Stanger BZ, et al.
1160 Single-cell lineage tracing of metastatic cancer reveals selection of hybrid EMT
1161 states. Cancer Cell. 2021 Aug 9;39(8):1150-1162.e9.

1162 84. Zhang Q, Fei L, Han R, Huang R, Wang Y, Chen H, et al. Single-cell
1163 transcriptome reveals cellular hierarchies and guides p-EMT-targeted trial in
1164 skull base chordoma. Cell Discov. 2022 Sep 20;8(1):94.

1165 85. Sullivan E, Harris M, Bhatnagar A, Guberman E, Zonfa I, Ravasz Regan E.
1166 Boolean modeling of mechanosensitive epithelial to mesenchymal transition
1167 and its reversal. iScience. 2023 Apr 21;26(4):106321.

1168 86. Schwab LP, Peacock DL, Majumdar D, Ingels JF, Jensen LC, Smith KD, et al.
1169 Hypoxia-inducible factor 1α promotes primary tumor growth and tumor-
1170 initiating cell activity in breast cancer. Breast Cancer Research. 2012 Jan
1171 7;14(1):R6.

1172 87. D'Uva G, Bertoni S, Lauriola M, De Carolis S, Pacilli A, D'Anello L, et al. Beta-
1173 Catenin/HuR Post-Transcriptional Machinery Governs Cancer Stem Cell
1174 Features in Response to Hypoxia. PLoS One. 2013 Nov 15;8(11):e80742.

1175 88. Yang MH, Wu MZ, Chiou SH, Chen PM, Chang SY, Liu CJ, et al. Direct
1176 regulation of TWIST by HIF-1alpha promotes metastasis. Nat Cell Biol. 2008
1177 Mar;10(3):295–305.

1178 89. Lv Y, Chen C, Zhao B, Zhang X. Regulation of matrix stiffness on the epithelial-
1179 mesenchymal transition of breast cancer cells under hypoxia environment.
1180 Naturwissenschaften. 2017 Jun;104(5–6):38.

1181 90. Uchida T, Rossignol F, Matthay MA, Mounier R, Couette S, Clottes E, et al.
1182 Prolonged Hypoxia Differentially Regulates Hypoxia-inducible Factor (HIF)-1α
1183 and HIF-2α Expression in Lung Epithelial Cells: IMPLICATION OF NATURAL
1184 ANTISENSE HIF-1α*. Journal of Biological Chemistry. 2004 Apr
1185 9;279(15):14871–8.

1186 91. Kaidi A, Williams AC, Paraskeva C. Interaction between beta-catenin and HIF-1
1187 promotes cellular adaptation to hypoxia. Nat Cell Biol. 2007 Feb;9(2):210–7.

1188 92. Yeung SJ, Pan J, Lee MH. Roles of p53, Myc and HIF-1 in Regulating Glycolysis
1189 — the Seventh Hallmark of Cancer. Cell Mol Life Sci. 2008 Sep 3;65(24):3981.

1190 93. Horváthová J, Moravčík R, Matúšková M, Šišovský V, Boháč A, Zeman M.
1191 Inhibition of Glycolysis Suppresses Cell Proliferation and Tumor Progression In
1192 Vivo: Perspectives for Chronotherapy. Int J Mol Sci. 2021 Apr 22;22(9):4390.

1193 94. Belapurkar R, Pfisterer M, Dreute J, Werner S, Zukunft S, Fleming I, et al. A
1194 transient increase of HIF-1α during the G1 phase (G1-HIF) ensures cell survival
1195 under nutritional stress. Cell Death Dis. 2023 Jul 27;14(7):1–15.

1196 95. Green SL, Freiberg RA, Giaccia AJ. p21(Cip1) and p27(Kip1) regulate cell cycle
1197 reentry after hypoxic stress but are not necessary for hypoxia-induced arrest.
1198 Mol Cell Biol. 2001 Feb;21(4):1196–206.

1199 96. Luo Y, Li M, Zuo X, Basourakos SP, Zhang J, Zhao J, et al. β-catenin nuclear
1200 translocation induced by HIF-1α overexpression leads to the radioresistance of
1201 prostate cancer. Int J Oncol. 2018 Jun;52(6):1827–40.

1202 97. Cummins EP, Berra E, Comerford KM, Ginouves A, Fitzgerald KT, Seeballuck F,
1203 et al. Prolyl hydroxylase-1 negatively regulates IκB kinase-β, giving insight into
1204 hypoxia-induced NFκB activity. Proc Natl Acad Sci U S A. 2006 Nov
1205 28;103(48):18154–9.

1206 98. McMahon S, Grondin F, McDonald PP, Richard DE, Dubois CM. Hypoxia-
1207 enhanced expression of the proprotein convertase furin is mediated by
1208 hypoxia-inducible factor-1: impact on the bioactivation of proproteins. J Biol
1209 Chem. 2005 Feb 25;280(8):6561–9.

1210 99. Matsuoka J, Yashiro M, Doi Y, Fuyuhiro Y, Kato Y, Shinto O, et al. Hypoxia
1211 Stimulates the EMT of Gastric Cancer Cells through Autocrine TGFβ Signaling.
1212 PLOS ONE. 2013 May 17;8(5):e62310.

1213 100. Mallikarjuna P, Raviprakash TS, Aripaka K, Ljungberg B, Landström M.
1214 Interactions between TGF-β type I receptor and hypoxia-inducible factor-α
1215 mediates a synergistic crosstalk leading to poor prognosis for patients with
1216 clear cell renal cell carcinoma. Cell Cycle. 2019 Jul 24;18(17):2141–56.

1217 101. Brereton CJ, Yao L, Davies ER, Zhou Y, Vukmirovic M, Bell JA, et al.
1218 Pseudohypoxic HIF pathway activation dysregulates collagen structure-function
1219 in human lung fibrosis. eLife. 11:e69348.

1220 102. Muñoz-Nájar UM, Neurath KM, Vumbaca F, Claffey KP. Hypoxia stimulates
1221 breast carcinoma cell invasion through MT1-MMP and MMP-2 activation.
1222 Oncogene. 2006 Apr 13;25(16):2379–92.

1223 103. Choi JY, Jang YS, Min SY, Song JY. Overexpression of MMP-9 and HIF-1α in
1224 Breast Cancer Cells under Hypoxic Conditions. J Breast Cancer. 2011
1225 Jun;14(2):88–95.

1226 104. Park JS, Burckhardt CJ, Lazcano R, Solis LM, Isogai T, Li L, et al. Mechanical
1227 regulation of glycolysis via cytoskeleton architecture. Nature. 2020
1228 Feb;578(7796):621–6.

1229 105. Gizak A, Wiśniewski J, Heron P, Mamczur P, Sygusch J, Rakus D. Targeting a
1230 moonlighting function of aldolase induces apoptosis in cancer cells. Cell Death
1231 Dis. 2019 Sep 26;10(10):712.

1232 106. van Leeuwaarde RS, Ahmad S, van Nesselrooij B, Zandee W, Giles RH. Von
1233 Hippel-Lindau Syndrome. In: Adam MP, Feldman J, Mirzaa GM, Pagon RA,
1234 Wallace SE, Bean LJ, et al., editors. GeneReviews® [Internet]. Seattle (WA):
1235 University of Washington, Seattle; 1993 [cited 2024 Jan 25]. Available from:
1236 http://www.ncbi.nlm.nih.gov/books/NBK1463/

1237 107. Ferlay J, Colombet M, Soerjomataram I, Dyba T, Randi G, Bettio M, et al.
1238 Cancer incidence and mortality patterns in Europe: Estimates for 40 countries
1239 and 25 major cancers in 2018. Eur J Cancer. 2018 Nov;103:356–87.

1240 108. Clark PE. The role of VHL in clear-cell renal cell carcinoma and its relation to
1241 targeted therapy. Kidney International. 2009 Nov 1;76(9):939–45.

1242 109. Pritchett TL, Bader HL, Henderson J, Hsu T. Conditional inactivation of the
1243 mouse von Hippel–Lindau tumor suppressor gene results in wide-spread
1244 hyperplastic, inflammatory and fibrotic lesions in the kidney. Oncogene. 2015
1245 May;34(20):2631–9.

1246 110. Wang SS, Gu YF, Wolff N, Stefanius K, Christie A, Dey A, et al. Bap1 is
1247 essential for kidney function and cooperates with Vhl in renal tumorigenesis.
1248 Proceedings of the National Academy of Sciences. 2014 Nov
1249 18;111(46):16538–43.

1250 111. Xu Z, Liu L, Jiang W, Qiu Y, Zhang B, Cheng J, et al. VHL missense mutation
1251 delineate aggressive clear cell renal cell carcinoma subtype with favorable
1252 immunotherapeutic response. J Immunother Cancer. 2024 Oct
1253 23;12(10):e009963.

1254 112. Gordan JD, Lal P, Dondeti VR, Letrero R, Parekh KN, Oquendo CE, et al. HIF-α
1255 Effects on c-Myc Distinguish Two Subtypes of Sporadic VHL-Deficient Clear Cell
1256 Renal Carcinoma. Cancer Cell. 2008 Dec 9;14(6):435–46.

1257 113. Lin PH, Huang CY, Yu KJ, Kan HC, Liu CY, Chuang CK, et al. Genomic
1258 characterization of clear cell renal cell carcinoma using targeted gene
1259 sequencing. Oncol Lett. 2021 Feb;21(2):169.

1260 114. Adeshakin FO, Adeshakin AO, Afolabi LO, Yan D, Zhang G, Wan X. Mechanisms
1261 for Modulating Anoikis Resistance in Cancer and the Relevance of Metabolic
1262 Reprogramming. Front Oncol. 2021 Mar 29;11:626577.

1263 115. Dong Z, Wang JZ, Yu F, Venkatachalam MA. Apoptosis-Resistance of Hypoxic
1264 Cells. Am J Pathol. 2003 Aug;163(2):663–71.

1265 116. Park SH, Riley P, Frisch SM. Regulation of anoikis by Deleted in Breast Cancer-
1266 1 (DBC1) through NF-κB. Apoptosis. 2013 Aug;18(8):949–62.

1267 117. Wang CY, Guttridge DC, Mayo MW, Baldwin AS. NF-κB Induces Expression of
1268 the Bcl-2 Homologue A1/Bfl-1 To Preferentially Suppress Chemotherapy-
1269 Induced Apoptosis. Mol Cell Biol. 1999 Sep;19(9):5923–9.

1270 118. Tilghman RW, Cowan CR, Mih JD, Koryakina Y, Gioeli D, Slack-Davis JK, et al.
1271 Matrix Rigidity Regulates Cancer Cell Growth and Cellular Phenotype. PLOS
1272 ONE. 2010 Sep 23;5(9):e12905.

1273 119. Mittal V. Epithelial Mesenchymal Transition in Tumor Metastasis. Annu Rev
1274 Pathol. 2018 Jan 24;13:395–412.

1275 120. Deritei D, Anamika WJ, Zhou X, Silverman EK, Regan ER, Glass K. HHIP's
1276 Dynamic Role in Epithelial Wound Healing Reveals a Potential Mechanism of
1277 COPD Susceptibility [Internet]. bioRxiv; 2024 [cited 2024 Dec 18]. p.
1278 2024.09.05.611545. Available from:
1279 https://www.biorxiv.org/content/10.1101/2024.09.05.611545v2

1280 121. Kai F, Drain AP, Weaver VM. The extracellular matrix modulates the metastatic
1281 journey. Dev Cell. 2019 May 6;49(3):332–46.

1282 122. Nguyen LK, Cavadas MAS, Scholz CC, Fitzpatrick SF, Bruning U, Cummins EP,
1283 et al. A dynamic model of the hypoxia-inducible factor 1α (HIF-1α) network.
1284 Journal of Cell Science. 2013 Mar 15;126(6):1454–63.

1285 123. Qutub AA, Popel AS. A computational model of intracellular oxygen sensing by
1286 hypoxia-inducible factor HIF1α. J Cell Sci. 2006 Aug 15;119(Pt 16):3467–80.

1287 124. Hashemzadeh S, Shahmorad S, Rafii-Tabar H, Omidi Y. Computational
1288 modeling to determine key regulators of hypoxia effects on the lactate
1289 production in the glycolysis pathway. Sci Rep. 2020 Jun 8;10(1):9163.

1290 125. Oliveira RH de M, Annex BH, Popel AS. Endothelial cells signaling and
1291 patterning under hypoxia: a mechanistic integrative computational model
1292 including the Notch-Dll4 pathway. Front Physiol [Internet]. 2024 Feb 22 [cited
1293 2024 Dec 18];15. Available from:
1294 https://www.frontiersin.org/journals/physiology/articles/10.3389/fphys.2024.1
1295 351753/full

1296 126. Hanahan D. Hallmarks of Cancer: New Dimensions. Cancer Discovery. 2022
1297 Jan 12;12(1):31–46.

1298 127. Kierans SJ, Taylor CT. Regulation of glycolysis by the hypoxia-inducible factor
1299 (HIF): implications for cellular physiology. The Journal of Physiology.
1300 2021;599(1):23–37.

1301 128. Gordan JD, Bertovrt JA, Hu CJ, Diehl JA, Simon MC. HIF-2α promotes hypoxic
1302 cell proliferation by enhancing c-Myc transcriptional activity. Cancer Cell. 2007
1303 Apr;11(4):335–47.

1304 129. Zhu C, Yu J, Pan Q, Yang J, Hao G, Wang Y, et al. Hypoxia-inducible factor-2
1305 alpha promotes the proliferation of human placenta-derived mesenchymal stem
1306 cells through the MAPK/ERK signaling pathway. Sci Rep. 2016 Oct
1307 21;6(1):35489.

1308 130. Ma X, Zhang H, Xue X, Shah YM. Hypoxia-inducible factor 2α (HIF-2α)
1309 promotes colon cancer growth by potentiating Yes-associated protein 1 (YAP1)
1310 activity. Journal of Biological Chemistry. 2017 Oct 13;292(41):17046–56.

1311 131. Chen SH, Xu LY, Wu YP, Ke ZB, Huang P, Lin F, et al. Tumor volume: a new
1312 prognostic factor of oncological outcome of localized clear cell renal cell
1313 carcinoma. BMC Cancer. 2021 Jan 19;21(1):79.

1314 132. Chrabańska M, Szweda-Gandor N, Drozdzowska B. Two Single Nucleotide
1315 Polymorphisms in the Von Hippel-Lindau Tumor Suppressor Gene in Patients
1316 with Clear Cell Renal Cell Carcinoma. Int J Mol Sci. 2023 Feb 14;24(4):3778.

1317 133. Stone RC, Pastar I, Ojeh N, Chen V, Liu S, Garzon KI, et al. Epithelial-
1318 Mesenchymal Transition in Tissue Repair and Fibrosis. Cell Tissue Res. 2016
1319 Sep;365(3):495–506.

1320 134. Lin Q, Cong X, Yun Z. Differential hypoxic regulation of hypoxia-inducible
1321 factors 1α and 2α. Mol Cancer Res. 2011 Jun;9(6):757–65.

1322 135. Zhang P, Yao Q, Lu L, Li Y, Chen PJ, Duan C. Hypoxia-Inducible Factor 3 Is an
1323 Oxygen-Dependent Transcription Activator and Regulates a Distinct
1324 Transcriptional Response to Hypoxia. Cell Reports. 2014 Mar 27;6(6):1110–21.

1325 136. Augstein A, Poitz DM, Braun-Dullaeus RC, Strasser RH, Schmeisser A. Cell-
1326 specific and hypoxia-dependent regulation of human HIF-3α: inhibition of the
1327 expression of HIF target genes in vascular cells. Cell Mol Life Sci. 2011 Aug
1328 1;68(15):2627–42.

1329 137. Sizek H, Deritei D, Fleig K, Harris M, Regan PL, Glass K, et al. Unlocking
1330 Mitochondrial Dysfunction-Associated Senescence (MiDAS) with NAD+ – a
1331 Boolean Model of Mitochondrial Dynamics and Cell Cycle Control. Tansl Onc.
1332 2023 Dec 1;(submitted).

1333 138. Kang H, Kim H, Lee S, Youn H, Youn B. Role of Metabolic Reprogramming in
1334 Epithelial–Mesenchymal Transition (EMT). Int J Mol Sci. 2019 Apr
1335 25;20(8):2042.

1336 139.Hong CF, Chen WY, Wu CW. Upregulation of Wnt signaling under hypoxia
1337 promotes lung cancer progression. Oncol Rep. 2017 Sep;38(3):1706–14.

1338 140.Shen X, Li M, Wang C, Liu Z, Wu K, Wang A, et al. Hypoxia is fine-tuned by Hif-
1339 1α and regulates mesendoderm differentiation through the Wnt/β-Catenin
1340 pathway. BMC Biol. 2022 Oct 5;20(1):219.

1341 141.Guo M, Niu Y, Xie M, Liu X, Li X. Notch signaling, hypoxia, and cancer. Front
1342 Oncol. 2023 Jan 31;13:1078768.

1343 142.Gyamfi J, Lee YH, Eom M, Choi J. Interleukin-6/STAT3 signalling regulates
1344 adipocyte induced epithelial-mesenchymal transition in breast cancer cells. Sci
1345 Rep. 2018 Jun 11;8:8859.

1346 143.Zhang T, Yang J, Sun Y, Song J, Gao D, Huang S, et al. Interleukin-6 and
1347 Hypoxia Synergistically Promote EMT-Mediated Invasion in Epithelial Ovarian
1348 Cancer via the IL-6/STAT3/HIF-1α Feedback Loop. Anal Cell Pathol (Amst).
1349 2023 Feb 13;2023:8334881.

1350 144.Li X, Kimura H, Hirota K, Kasuno K, Torii K, Okada T, et al. Synergistic effect of
1351 hypoxia and TNF-α on production of PAI-1 in human proximal renal tubular
1352 cells. Kidney International. 2005 Aug 1;68(2):569–83.

1353 145.Basu S, Cheriyamundath S, Ben-Ze'ev A. Cell–cell adhesion: linking Wnt/β-
1354 catenin signaling with partial EMT and stemness traits in tumorigenesis.
1355 F1000Res. 2018 Sep 18;7:F1000 Faculty Rev-1488.

1356 146.Katoh Y, Katoh M. Hedgehog signaling, epithelial-to-mesenchymal transition
1357 and miRNA (review). Int J Mol Med. 2008 Sep;22(3):271–5.

1358 147.Deshmukh AP, Vasaikar SV, Tomczak K, Tripathi S, den Hollander P, Arslan E,
1359 et al. Identification of EMT signaling cross-talk and gene regulatory networks
1360 by single-cell RNA sequencing. Proceedings of the National Academy of
1361 Sciences. 2021 May 11;118(19):e2102050118.

1362 148.Shaul ME, Fridlender ZG. Tumour-associated neutrophils in patients with
1363 cancer. Nat Rev Clin Oncol. 2019 Oct;16(10):601–20.

1364 149.Doak GR, Schwertfeger KL, Wood DK. Distant Relations: Macrophage Functions
1365 in the Metastatic Niche. Trends in Cancer. 2018 Jun 1;4(6):445–59.

1366 150.Schlesinger M. Role of platelets and platelet receptors in cancer metastasis. J
1367 Hematol Oncol. 2018 Oct 11;11(1):125.

1368 151.Gaggioli C, Hooper S, Hidalgo-Carcedo C, Grosse R, Marshall JF, Harrington K,
1369 et al. Fibroblast-led collective invasion of carcinoma cells with differing roles for
1370 RhoGTPases in leading and following cells. Nat Cell Biol. 2007 Dec;9(12):1392–
1371 400.

1372 152. Guo Y, Cui W, Pei Y, Xu D. Platelets promote invasion and induce epithelial to
1373 mesenchymal transition in ovarian cancer cells by TGF-β signaling pathway.
1374 Gynecologic Oncology. 2019 Jun;153(3):639–50.

1375 153. Nacarelli T, Lau L, Fukumoto T, Zundell J, Fatkhutdinov N, Wu S, et al. NAD+
1376 metabolism governs the proinflammatory senescence-associated secretome.
1377 Nat Cell Biol. 2019 Mar;21(3):397–407.

1378 154. Smit MA, Peeper DS. Epithelial-mesenchymal transition and senescence: two
1379 cancer-related processes are crossing paths. Aging (Albany NY). 2010 Oct
1380 17;2(10):735–41.

1381 155. Liu Y, El-Naggar S, Darling DS, Higashi Y, Dean DC. ZEB1 Links Epithelial-
1382 Mesenchymal Transition and Cellular Senescence. Development. 2008
1383 Feb;135(3):579–88.

1384 156. Malik-Sheriff RS, Glont M, Nguyen TVN, Tiwari K, Roberts MG, Xavier A, et al.
1385 BioModels-15 years of sharing computational models in life science. Nucleic
1386 Acids Res. 2020 Jan 8;48(D1):D407–15.

1387 157. Chaouiya C, Naldi A, Thieffry D. Logical modelling of gene regulatory networks
1388 with GINsim. Methods Mol Biol. 2012;804:463–79.

1389 158. Helikar T, Kowal B, McClenathan S, Bruckner M, Rowley T, Madrahimov A, et
1390 al. The Cell Collective: toward an open and collaborative approach to systems
1391 biology. BMC Syst Biol. 2012 Aug 7;6:96.

1392 159. Albert I, Thakar J, Li S, Zhang R, Albert R. Boolean network simulations for life
1393 scientists. Source Code Biol Med. 2008 Nov 14;3:16.

1394 160. yWorks GmbH. yEd [Internet]. 2019. Available from:
1395 https://www.yworks.com/products/yed

1396 161. Mann M, Klemm K. Efficient exploration of discrete energy landscapes. Physical
1397 Review E. 2009 Oct;83(1):011113.

1398 162. Deritei D, Aird WC, Ercsey-Ravasz M, Regan ER. Principles of dynamical
1399 modularity in biological regulatory networks. Sci Rep. 2016 Mar 16;6:21957.

1400 163. Sizek H, Hamel A, Deritei D, Campbell S, Ravasz Regan E. Boolean model of
1401 growth signaling, cell cycle and apoptosis predicts the molecular mechanism of
1402 aberrant cell cycle progression driven by hyperactive PI3K. PLoS Comput Biol.
1403 2019;15(3):e1006402.

1404 164. Guberman E, Sherief H, Regan ER. Boolean model of anchorage dependence
1405 and contact inhibition points to coordinated inhibition but semi-independent
1406 induction of proliferation and migration. Comput Struct Biotechnol J.
1407 2020;18:2145–65.

1408
1409

1410 # Supplementary Figures

1411 **SM Figure 1.** Hif-1α is required for proliferation under normoxia (full version of Fig. 2A).

1412 **SM Figure 2.** Hif-1α hyper-activation blocks the cell cycle by repressing Myc.

1413 **SM Figure 3.** Hypoxia induces EMT independently of TFG-β.

1414 **SM Figure 4.** A stiff ECM aids hypoxia-induced EMT, compared to hybrid E/M under
1415 normoxia.

1416 **SM Figure 5.** ECM stiffness boosts both hypoxia- and TGF-β-induced EMT; high levels
1417 of both are required to drive EMT on very soft ECMs.

1418 **SM Figure 6.** VHL deficiency boosts bio mechanically induced EMT in normoxia as well
1419 as hypoxia at moderate ECM stiffness and medium-high density, but abolishes cell
1420 cycle entry.

1421 **SM Figure 7.** VHL deficiency-induced cell cycle arrest is broken by cooperative hyper-
1422 activation of Myc and Cyclin D.

1423 **SM Figure 8.** Hypoxia confers anoikis resistance and protection from TGF-β induced
1424 epithelial cell apoptosis on a soft ECM (full version of Fig. 5).

1425 **SM Figure 9.** Saturating autocrine TGF-β signaling protects all mesenchymal cells from
1426 anoikis, but also blocks MET on a stiff ECM.

1427 **SM Figure 10.** Slight breaks in the autocrine TGF-β signaling loop are potent inducers
1428 of anoikis and apoptosis on soft ECM.

SM Figure 11. A changing mix of model cell phenotypes as a function of mitogen, cell density, ECM stiffness and hypoxia allows us to track TME-driven EMT and MET during the metastatic cascade.

Supplementary Tables

SM Table 1. Description and experimental support for all nodes and links of the Boolean Regulatory network model in Fig. 1C.

SM Table 2. List of 150 published experimental assays used for model validation, marked to indicate success/failure of the model in replicating each assay.

Supplementary Files

SM File 1. Files read by *dynmod* to simulate the Boolean model's behaviors. These include the model in .dmms format (as well as .BooleanNet and .SBML formats, namely *Hypoxia_EMT_Model.dmms*, *Hypoxia_EMT_Model.booleannet, Hypoxia_EMT_Model.sbml*), the "in silico protocol" files for reproducing all figures (*Hypoxia_EMT_Main_Fig.vex, Hypoxia_EMT_SM_Fig.vex*) and the model network in .graphml format (*Hypoxia_EMT_Model.graphml*).

SM File 2. Files read by *dynmod* to simulate the isolated EMT module. These include the EMT module model in .dmms format (*EMT_module_Hypoxia.dmms*) and an "in silico protocol" file for generating time courses to check the module's attractors (*EMT_Module.vex*).

SM File 3. Files read by *dynmod* to rerun all model validation experiments (*Hypoxia_EMT_Validation.vex*), the Pyhton3 script and .csv file that performs statistical

tests on the simulation results, summarizes them, and generates the figures SM File 4 (*Hypoxia Model Validation Script.py, ST2 - Hypoxia model validation list.csv*).

SM File 4. Auto-generated validation figures (150 panels with statistical tests, marked for match / mismatch with expediting data).

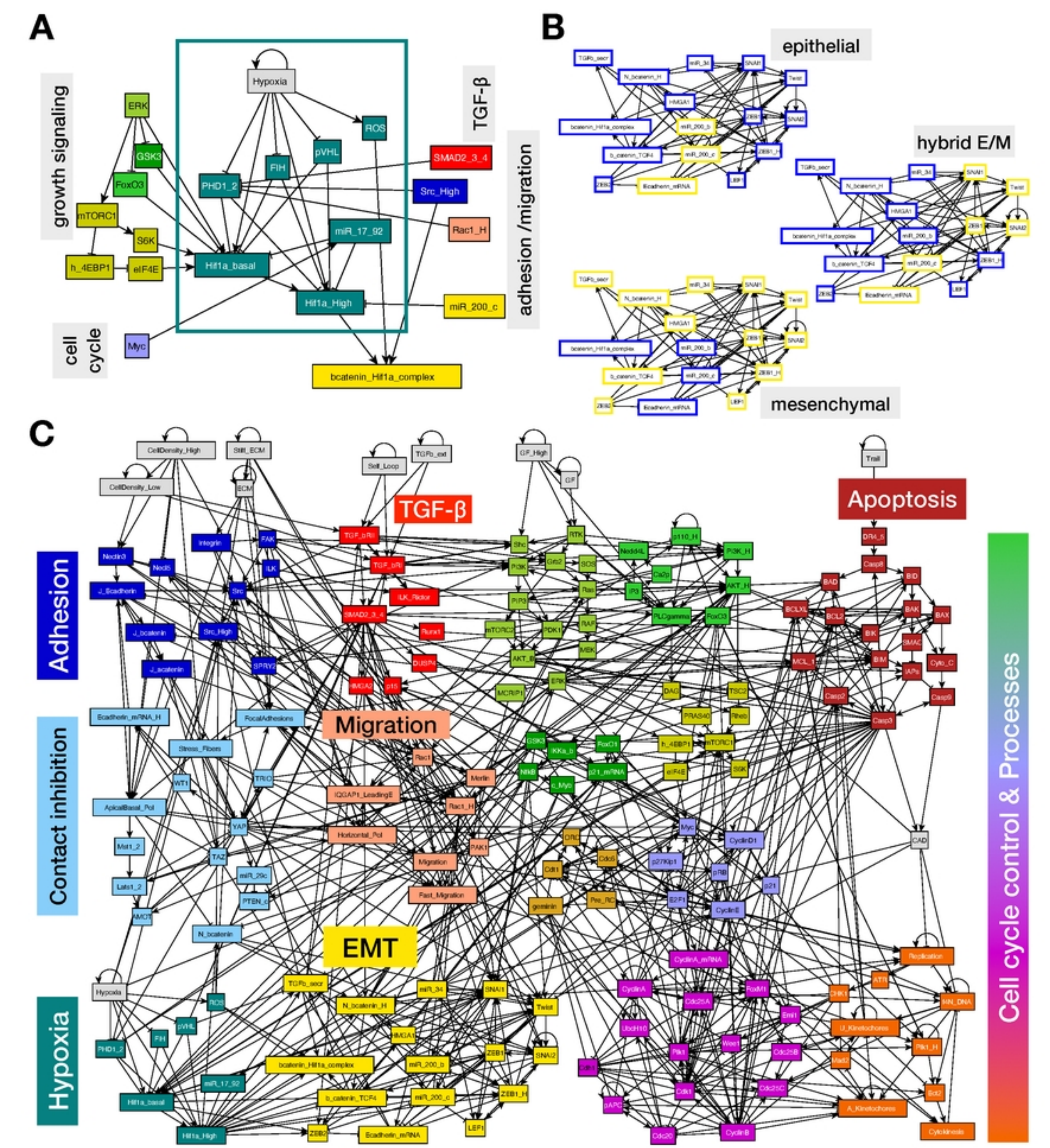
A
growth signaling
ERK
GSK3
FoxO3
mTORC1
S6K
h_4EBP1
eIF4E
cell cycle
Myc
Hypoxia
ROS
pVHL
FIH
PHD1_2
SMAD2_3_4
Src_High
Rac1_H
miR_17_92
Hif1a_basal
Hif1a_High
miR_200_c
bcatenin_Hif1a_complex
TGF-β
adhesion /migration
B
epithelial
hybrid E/M
mesenchymal
C
TGF-β
Apoptosis
Adhesion
Contact inhibition
Hypoxia
Migration
EMT
Cell cycle control & Processes

Figure 1

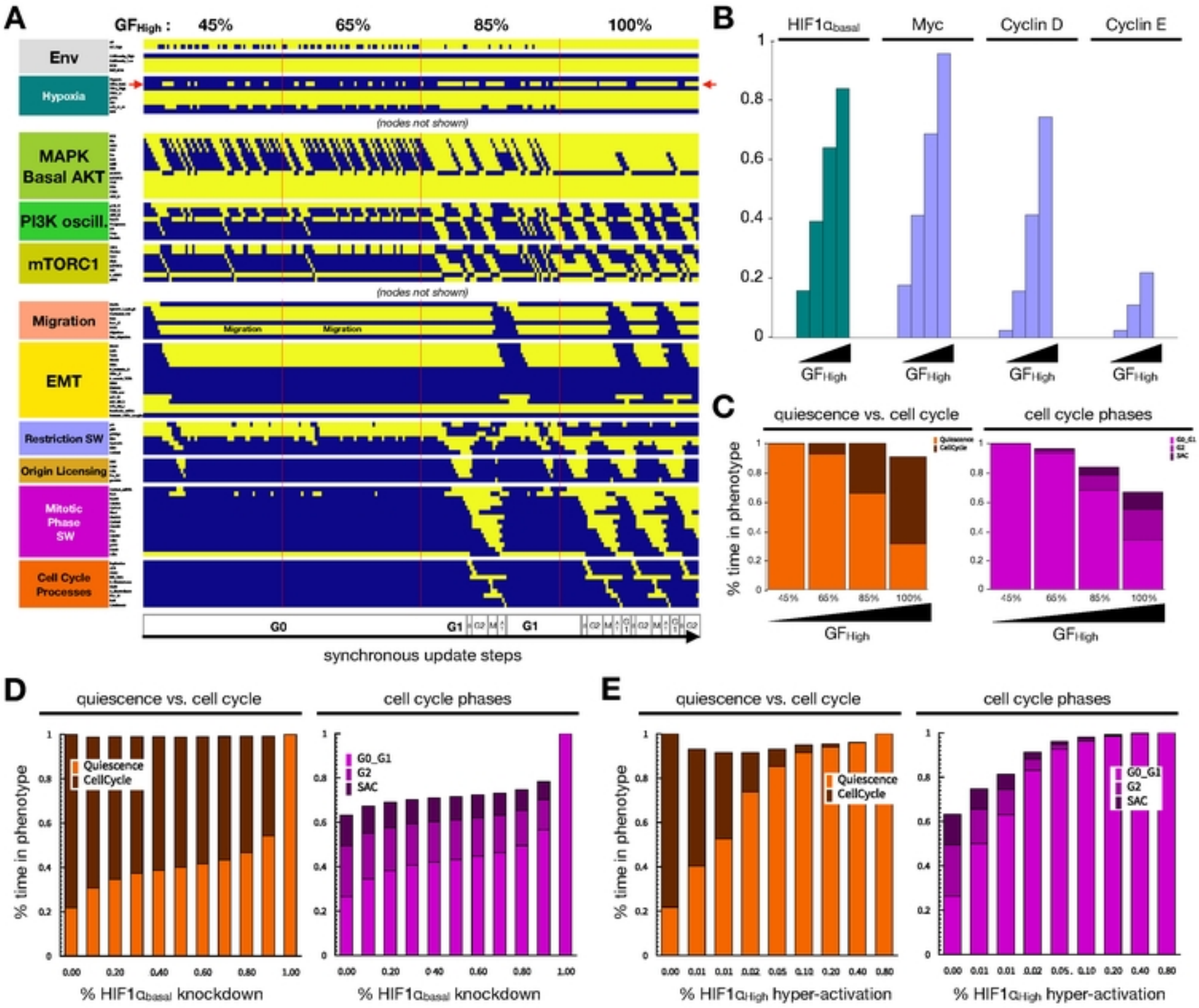
A
GFHigh : 45% 65% 85% 100%
Env
Hypoxia
(nodes not shown)
MAPK Basal AKT
PI3K oscill.
mTORC1
(nodes not shown)
Migration
EMT
Restriction SW
Origin Licensing
Mitotic Phase SW
Cell Cycle Processes
G0
G1
G1
synchronous update steps
B
HIF1αbasal
Myc
Cyclin D
Cyclin E
GFHigh
C
quiescence vs. cell cycle
cell cycle phases
% time in phenotype
GFHigh
D
quiescence vs. cell cycle
cell cycle phases
Quiescence
CellCycle
G0_G1
G2
SAC
% time in phenotype
% HIF1αbasal knockdown
E
quiescence vs. cell cycle
cell cycle phases
% time in phenotype
% HIF1αHigh hyper-activation

Figure 2

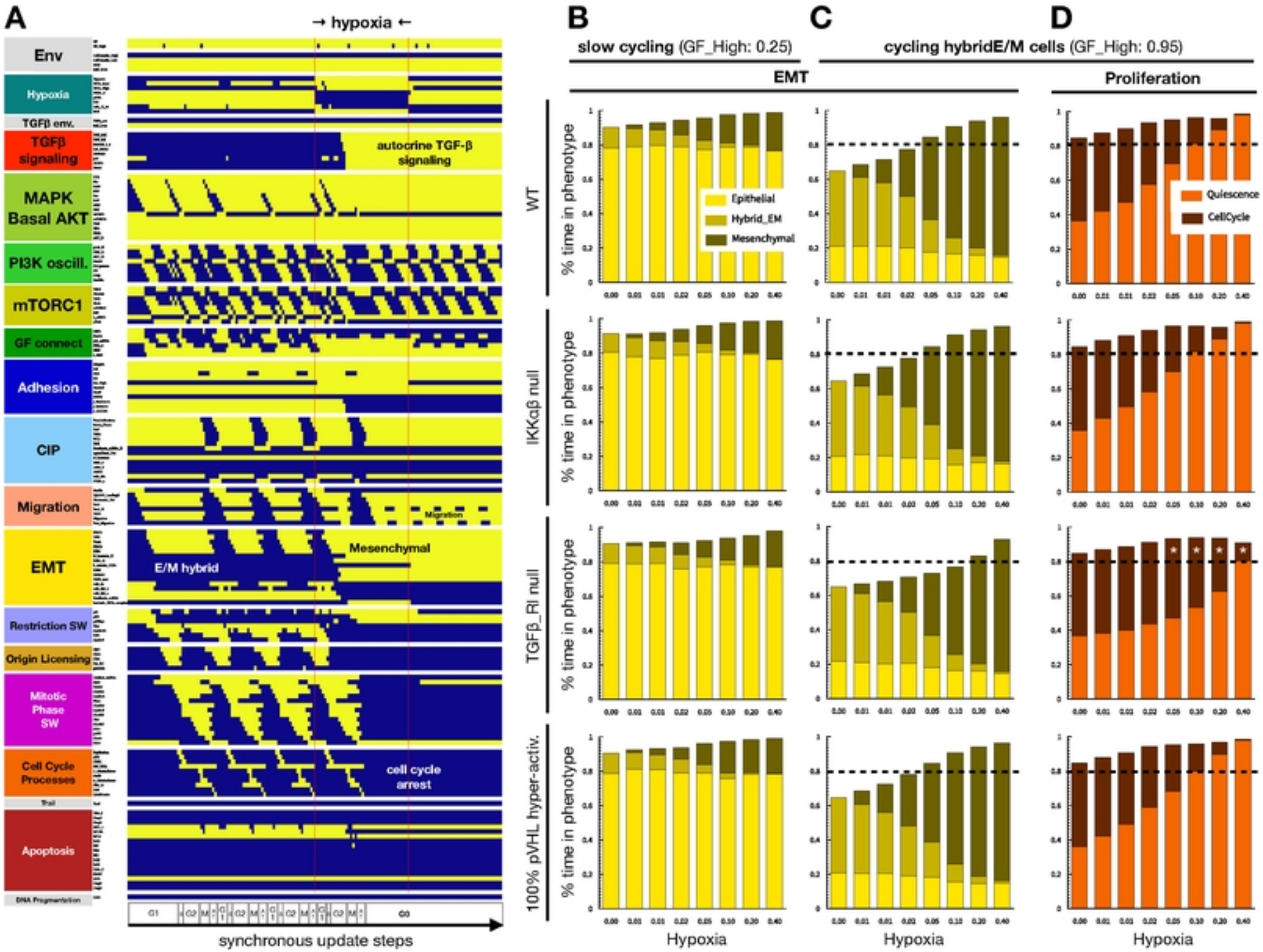
A
→ hypoxia ←
Env
Hypoxia
TGFβ env.
TGFβ signaling
autocrine TGF-β signaling
MAPK Basal AKT
PI3K oscill.
mTORC1
GF connect
Adhesion
CIP
Migration
Migration
EMT
Mesenchymal
E/M hybrid
Restriction SW
Origin Licensing
Mitotic Phase SW
Cell Cycle Processes
cell cycle arrest
Apoptosis
synchronous update steps
B
slow cycling (GF_High: 0.25)
C
D
cycling hybridE/M cells (GF_High: 0.95)
EMT
Proliferation
WT
IKKαβ null
TGFβ_RI null
100% pVHL hyper-activ.
% time in phenotype
Epithelial
Hybrid_EM
Mesenchymal
Quiescence
CellCycle
Hypoxia

Figure 3

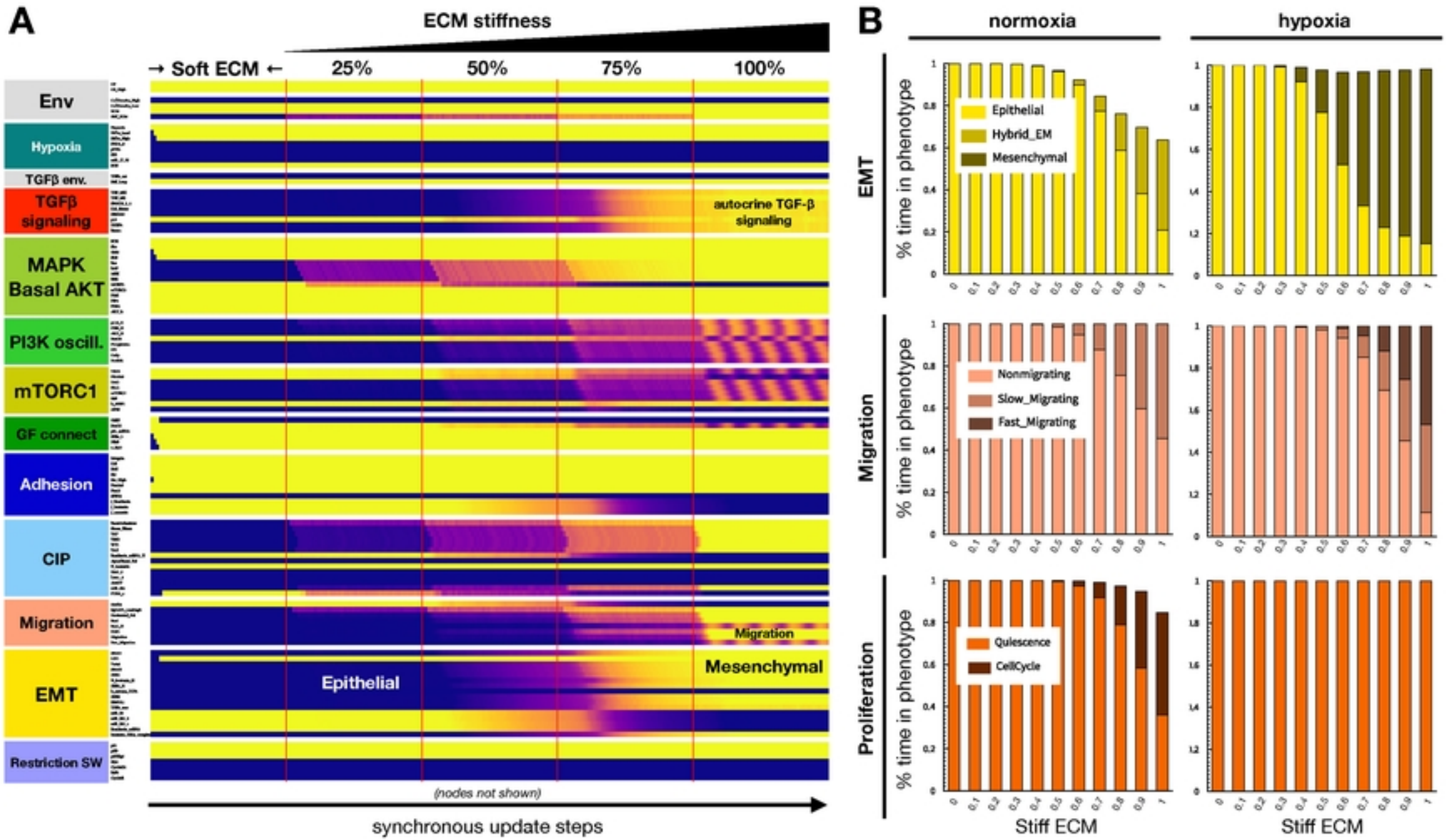
A
ECM stiffness
→ Soft ECM ←
25%
50%
75%
100%
Env
Hypoxia
TGFβ env.
TGFβ signaling
autocrine TGF-β signaling
MAPK Basal AKT
PI3K oscill.
mTORC1
GF connect
Adhesion
CIP
Migration
Migration
EMT
Epithelial
Mesenchymal
Restriction SW
(nodes not shown)
synchronous update steps
B
normoxia
hypoxia
EMT
% time in phenotype
Epithelial
Hybrid_EM
Mesenchymal
Migration
% time in phenotype
Nonmigrating
Slow_Migrating
Fast_Migrating
Proliferation
% time in phenotype
Quiescence
CellCycle
Stiff ECM
Stiff ECM

Figure 4

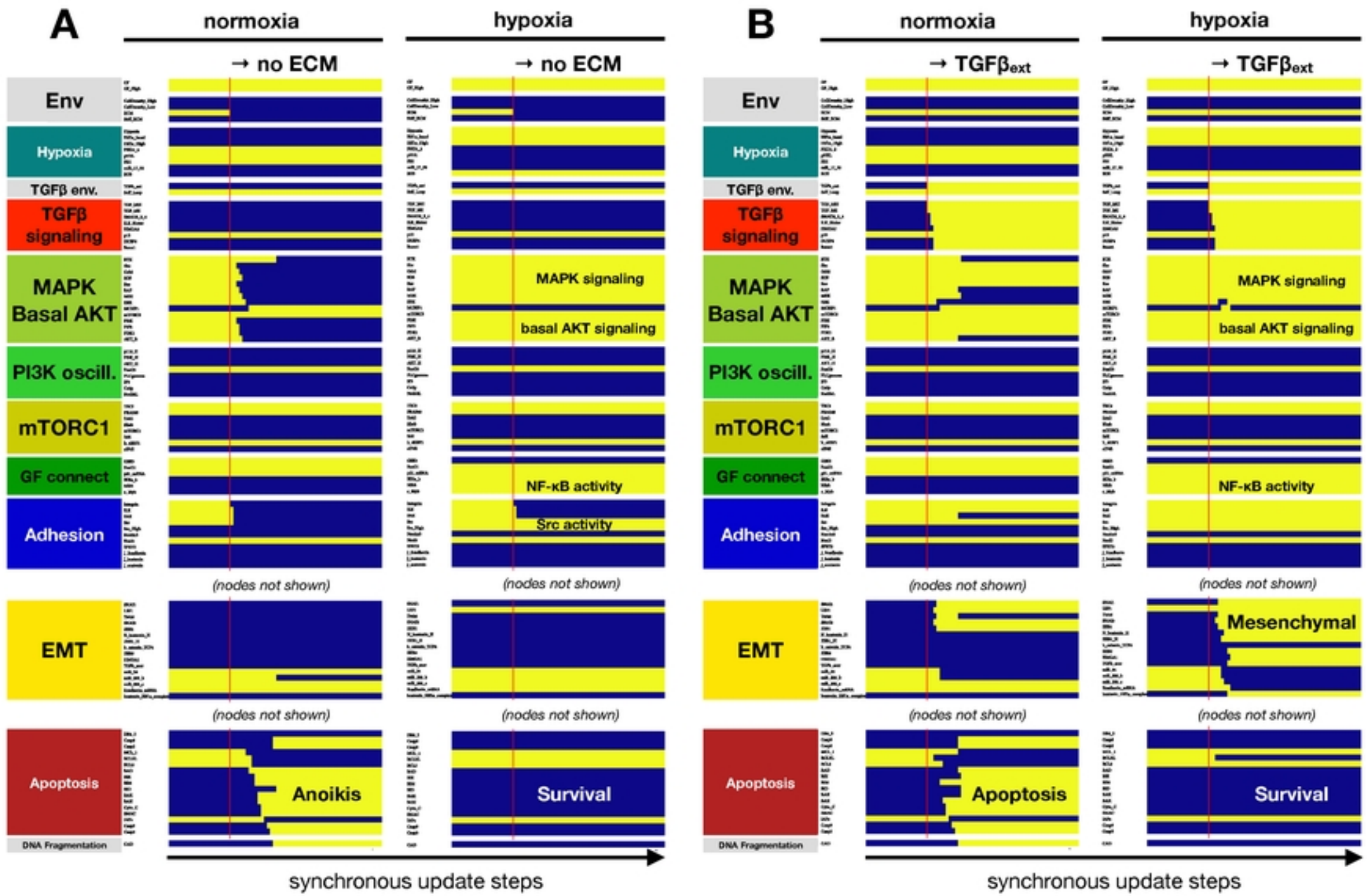
A
normoxia
hypoxia
→ no ECM
→ no ECM
Env
Hypoxia
TGFβ env.
TGFβ signaling
MAPK Basal AKT
MAPK signaling
basal AKT signaling
PI3K oscill.
mTORC1
GF connect
NF-κB activity
Adhesion
Src activity
(nodes not shown)
(nodes not shown)
EMT
(nodes not shown)
(nodes not shown)
Apoptosis
Anoikis
Survival
DNA Fragmentation
synchronous update steps
B
normoxia
hypoxia
→ TGFβext
→ TGFβext
Env
Hypoxia
TGFβ env.
TGFβ signaling
MAPK Basal AKT
MAPK signaling
basal AKT signaling
PI3K oscill.
mTORC1
GF connect
NF-κB activity
Adhesion
(nodes not shown)
(nodes not shown)
EMT
Mesenchymal
(nodes not shown)
(nodes not shown)
Apoptosis
Apoptosis
Survival
DNA Fragmentation
synchronous update steps

Figure 5

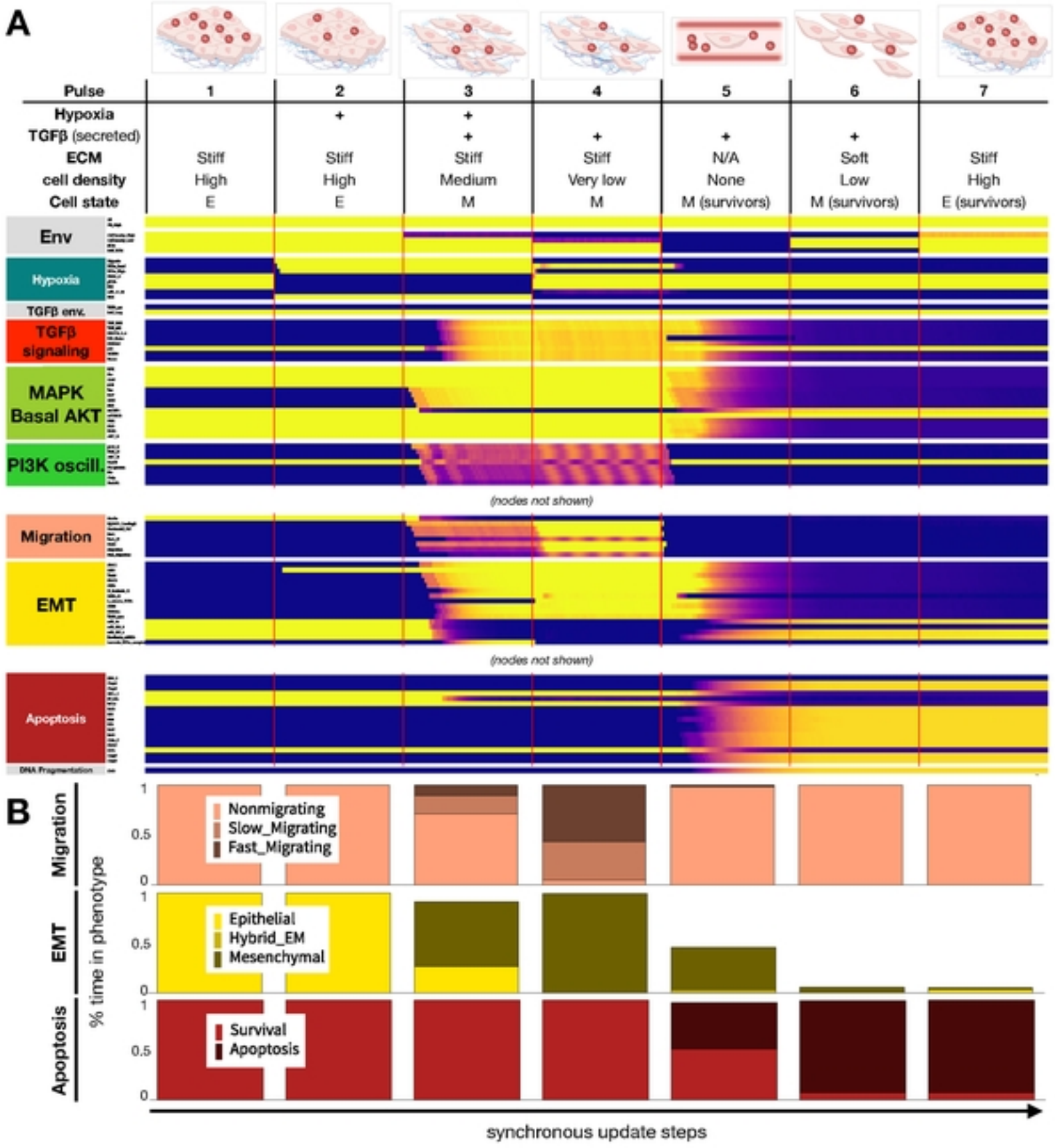
A
Pulse
1
2
3
4
5
6
7
Hypoxia
TGFβ (secreted)
ECM
cell density
Cell state
Stiff
High
E
Stiff
High
E
Stiff
Medium
M
Stiff
Very low
M
N/A
None
M (survivors)
Soft
Low
M (survivors)
Stiff
High
E (survivors)
Env
Hypoxia
TGFβ env.
TGFβ signaling
MAPK
Basal AKT
PI3K oscill.
(nodes not shown)
Migration
EMT
(nodes not shown)
Apoptosis
DNA Fragmentation
B
Migration
EMT
Apoptosis
% time in phenotype
Nonmigrating
Slow_Migrating
Fast_Migrating
Epithelial
Hybrid_EM
Mesenchymal
Survival
Apoptosis
synchronous update steps

Figure 6